



# **NAVAL POSTGRADUATE SCHOOL**

**MONTEREY, CALIFORNIA**

## **THESIS**

### **COMMAND WIRE SENSOR MEASUREMENTS**

by

Chin Liong Yeo

September 2012

Thesis Advisor:  
Second Reader:

David C. Jenn  
Tri T.Ha

**Approved for public release; distribution is unlimited**

THIS PAGE INTENTIONALLY LEFT BLANK

<b>REPORT DOCUMENTATION PAGE</b>			<i>Form Approved OMB No. 0704-0188</i>	
Public reporting burden for this collection of information is estimated to average 1 hour per response, including the time for reviewing instruction, searching existing data sources, gathering and maintaining the data needed, and completing and reviewing the collection of information. Send comments regarding this burden estimate or any other aspect of this collection of information, including suggestions for reducing this burden, to Washington headquarters Services, Directorate for Information Operations and Reports, 1215 Jefferson Davis Highway, Suite 1204, Arlington, VA 22202-4302, and to the Office of Management and Budget, Paperwork Reduction Project (0704-0188) WashingtonDC20503.				
<b>1. AGENCY USE ONLY (Leave blank)</b>		<b>2. REPORT DATE</b> September 2012	<b>3. REPORT TYPE AND DATES COVERED</b> Master's Thesis	
<b>4. TITLE AND SUBTITLE:</b> Command Wire Sensor Measurements			<b>5. FUNDING NUMBERS</b>	
<b>6. AUTHOR(S)</b> Chin Liong Yeo				
<b>7. PERFORMING ORGANIZATION NAME(S) AND ADDRESS(ES)</b> Naval Postgraduate School Monterey, CA93943-5000			<b>8. PERFORMING ORGANIZATION REPORT NUMBER</b>	
<b>9. SPONSORING /MONITORING AGENCY NAME(S) AND ADDRESS(ES)</b> N/A			<b>10. SPONSORING/MONITORING AGENCY REPORT NUMBER</b>	
<b>11. SUPPLEMENTARY NOTES:</b> The views expressed in this thesis are those of the author and do not reflect the official policy or position of the Department of Defense or the U.S. Government. IRB Protocol number N/A.				
<b>12a. DISTRIBUTION / AVAILABILITY STATEMENT</b> Approved for public release; distribution is unlimited			<b>12b. DISTRIBUTION CODE</b> A	
<b>13. ABSTRACT (maximum 200words)</b>  <p>After the recent success in jamming wireless improvised explosive devices (IEDs), the threat nowadays has shifted towards the use of buried command wires. A capability to immediately detect the presence of a command wire would be of great value to the troops on the ground. The major challenge of a command wire sensor is to detect the wire in clutter and achieve a high probability of detection without large number of false alarms. The objective of this thesis is to investigate the wire scattering behavior and clutter characteristics through measurements performed in the NPS anechoic chamber.</p> <p>The research has successfully resolved the various multipath components within the anechoic chamber. The transmit-receive coupling between the antennas was reduced through the appropriate use of absorbers. Various wire scattering and clutter characteristics were established through the measurement results. In addition, the measurement results have also demonstrated close-in clutter rejection by utilizing time gating.</p> <p>Recommendations for future work were proposed to gather more data to support the ongoing NPS research on the Command Wire Sensor design.</p>				
<b>14. SUBJECT TERMS</b> Command Wire Sensor, Wire Scattering, Time Gating			<b>15. NUMBER OF PAGES</b> 106	
			<b>16. PRICE CODE</b>	
<b>17. SECURITY CLASSIFICATION OF REPORT</b> Unclassified	<b>18. SECURITY CLASSIFICATION OF THIS PAGE</b> Unclassified	<b>19. SECURITY CLASSIFICATION OF ABSTRACT</b> Unclassified	<b>20. LIMITATION OF ABSTRACT</b> UU	

THIS PAGE INTENTIONALLY LEFT BLANK

**Approved for public release; distribution is unlimited**

**COMMAND WIRE SENSOR MEASUREMENTS**

Chin Liong Yeo  
Civilian, Singapore Technologies Kinetics  
B.S., University of Queensland, 2000

Submitted in partial fulfillment of the  
requirements for the degree of

**MASTER OF SCIENCE IN ELECTRICAL ENGINEERING**

from the

**NAVAL POSTGRADUATE SCHOOL  
September 2012**

Author: Chin Liong Yeo

Approved by: David C. Jenn  
Thesis Advisor

Tri T. Ha  
Second Reader

R. Clark Robertson  
Chair, Department of Electrical and Computer Engineering

THIS PAGE INTENTIONALLY LEFT BLANK

## **ABSTRACT**

After the recent success in jamming wireless improvised explosive devices (IEDs), the threat nowadays has shifted towards the use of buried command wires. A capability to immediately detect the presence of a command wire would be of great value to the troops on the ground. The major challenge of a command wire sensor is to detect the wire in clutter and achieve a high probability of detection without large number of false alarms. The objective of this thesis is to investigate the wire scattering behavior and clutter characteristics through measurements performed in the NPS anechoic chamber.

The research has successfully resolved the various multipath components within the anechoic chamber. The transmit-receive coupling between the antennas was reduced through the appropriate use of absorbers. Various wire scattering and clutter characteristics were established through the measurement results. In addition, the measurement results have also demonstrated close-in clutter rejection by utilizing time gating.

Recommendations for future work were proposed to gather more data to support the ongoing NPS research on the Command Wire Sensor design.

THIS PAGE INTENTIONALLY LEFT BLANK



## TABLE OF CONTENTS

<b>I.</b>	<b>INTRODUCTION.....</b>	<b>1</b>
<b>A.</b>	<b>BACKGROUND .....</b>	<b>1</b>
<b>B.</b>	<b>OBJECTIVE .....</b>	<b>3</b>
<b>C.</b>	<b>THESIS OUTLINE.....</b>	<b>4</b>
<b>II.</b>	<b>REVIEW OF PREVIOUS WORK.....</b>	<b>5</b>
<b>A.</b>	<b>EXISTING DETECTION SYSTEMS .....</b>	<b>5</b>
<b>B.</b>	<b>GROUND PENETRATING RADAR.....</b>	<b>6</b>
1.	GPR for Landmine Detection .....	6
2.	Attenuation .....	8
3.	Coupling Energy into the Ground.....	9
4.	Clutter .....	11
5.	Vehicle Based Radar Systems.....	11
<b>C.</b>	<b>SYNTHETIC APERTURE RADAR.....</b>	<b>11</b>
1.	Applications .....	12
2.	Change Detection .....	13
<b>D.</b>	<b>COMMAND WIRE SENSOR SYSTEM CHALLENGES.....</b>	<b>15</b>
1.	Wire Scattering .....	16
2.	Propagation and Frequency Considerations.....	17
3.	Clutter Characteristics .....	19
<b>E.</b>	<b>SUMMARY .....</b>	<b>19</b>
<b>III.</b>	<b>THEORY .....</b>	<b>21</b>
<b>A.</b>	<b>WIRE SCATTERING .....</b>	<b>21</b>
1.	Travelling Waves .....	21
2.	Scattering by a Straight Thin Wire.....	22
3.	Multipath .....	25
<b>B.</b>	<b>CLUTTER MODELING .....</b>	<b>25</b>
1.	Surface-clutter Radar Equation .....	26
2.	Signal-to-Clutter Ratio .....	28
3.	Total Clutter Power .....	29
<b>C.</b>	<b>TIME GATING.....</b>	<b>30</b>
1.	Radar Range Gating .....	30
2.	Time Gating for Wire Detection.....	31
<b>D.</b>	<b>PROBABILITIES OF DETECTION AND FALSE ALARM.....</b>	<b>31</b>
1.	Threshold Detection.....	31
2.	False Alarms .....	33
<b>E.</b>	<b>SIMULATION RESULT .....</b>	<b>33</b>
<b>F.</b>	<b>SUMMARY .....</b>	<b>35</b>
<b>IV.</b>	<b>MEASUREMENT RESULTS .....</b>	<b>37</b>
<b>A.</b>	<b>TEST SETUP .....</b>	<b>37</b>
1.	Chamber Dimensions.....	37

2.	Antenna Dimensions .....	38
3.	Equipment Setup.....	39
B.	BEAMWIDTH MEASUREMENTS .....	40
1.	Equipment Setup.....	40
2.	Beamwidth Plots.....	41
C.	HORN LEAKAGE.....	43
1.	Chamber Ambient .....	43
2.	Leakage Reduction.....	44
D.	WIRE SCATTERING MEASUREMENTS.....	48
1.	Initial Wire Measurements .....	48
2.	Plate Measurements.....	51
3.	Pole Measurements .....	53
E.	TIME GATING.....	55
1.	Time Gating Range .....	55
2.	Measurements with Time Gating .....	60
3.	Comparison Measurements .....	63
4.	Comparison Measurements without Background Subtraction.....	66
5.	Wire Returns versus Aspect Angle without Background Subtraction .....	68
F.	SUMMARY .....	76
V.	SUMMARY, CONCLUSIONS AND RECOMMENDATIONS .....	77
A.	SUMMARY AND CONCLUSIONS .....	77
B.	RECOMMENDATIONS.....	78
	LIST OF REFERENCES .....	81
	INITIAL DISTRIBUTION LIST .....	83

## LIST OF FIGURES

Figure 1.	The IED threat (From [2]).....	1
Figure 2.	Soldiers trying to uncover a command wire (From [3]) .....	2
Figure 3.	Husky mine detection vehicle with ground penetrating radar (From [10]) .....	6
Figure 4.	Propagation losses plotted against frequency for several values of $\tan \delta$ (After [4]).....	8
Figure 5.	Spectrum of transmitted and received signals after passing through lossy ground (After [4]) .....	9
Figure 6.	Parallel polarized wave incident on an interface at the Brewster angle (After [11]).....	10
Figure 7.	SAR mounted on the Predator UAV (From [16]).....	13
Figure 8.	Example of SAR CCD (From [16]) .....	14
Figure 9.	Vehicle mounted command wire sensor (From [7]) .....	15
Figure 10.	General sensor-wire geometry (From [7]) .....	17
Figure 11.	Travelling waves reflection (From [18]).....	21
Figure 12.	Geometry of straight wire (After [19]) .....	22
Figure 13.	Scattering contributions for a straight wire (After [19]).....	23
Figure 14.	Band limited impulse response for a wire at $\theta = 45^\circ$ (After [19]) .....	24
Figure 15.	Antenna beam geometry (From [7]) .....	26
Figure 16.	Backscatter from a differential ground patch (From [7]).....	29
Figure 17.	Time gating to reduce clutter (From [7]) .....	31
Figure 18.	Envelope of radar receiver output (From [14]).....	32
Figure 19.	Typical power contours for wire scattering at 300 MHz (From [7]) .....	34
Figure 20.	Typical power contours for wire scattering at 1 GHz (From [7]).....	35
Figure 21.	Specifications of the anechoic chamber at the Naval Postgraduate School (From [21]).....	37
Figure 22.	Transmit and receive horn dimensions .....	38
Figure 23.	Test equipment setup .....	39
Figure 24.	Antenna beamwidth measurement.....	40
Figure 25.	Antenna beamwidth at 4 GHz.....	41
Figure 26.	Antenna beamwidth at 5 GHz.....	42
Figure 27.	Antenna beamwidth at 6 GHz.....	42
Figure 28.	Anechoic chamber Ambient 4 – 6 GHz.....	43
Figure 29.	One piece of RAM inserted between Tx and Rx horns (front view).....	44
Figure 30.	Two pieces of RAM inserted between Tx and Rx horns (side view) .....	45
Figure 31.	Chamber ambient with one piece of RAM and without RAM .....	46
Figure 32.	Chamber ambient with two pieces of RAM foam and without RAM .....	46
Figure 33.	Chamber ambient with three pieces of RAM and without RAM .....	47
Figure 34.	Chamber ambient comparison for zero to three pieces of RAM .....	47
Figure 35.	Wire laid horizontally across the width of the chamber, five meters from the antenna .....	48
Figure 36.	RCS of a wire laid horizontally across the chamber, five meters from the antennas.....	49

Figure 37.	Wire hung vertically from the ceiling, six meters from the antenna .....	50
Figure 38.	Residual scattering from a wire hung vertically from the ceiling, six meters from the antenna.....	50
Figure 39.	Square metal plate placed on pedestal, six meters away from the antenna .....	51
Figure 40.	Measured return of 0.22 by 0.22 metal plate, placed six meters away from the antenna .....	52
Figure 41.	2.45 meter metal pole placed vertically, six meters away from the antenna ...	53
Figure 42.	Return from a 2.45 meter vertical pole, placed six meters away from the antenna .....	54
Figure 43.	Multipath components within anechoic chamber .....	54
Figure 44.	Time gated return for the plate six meters from the antenna, at 25 to 40 ns....	56
Figure 45.	Time gated return for the plate five meters from the antenna, at 20 to 30 ns..	56
Figure 46.	Time gated return for the plate four meters from the antenna, at 15 to 25 ns..	57
Figure 47.	Time gated return for the plate three meters from the antenna, at 10 to 20 ns.....	57
Figure 48.	Time gated return for the plate two meters from the antenna, at 0 to 10 ns ....	58
Figure 49.	Time gated return for the plate one meter from the antenna, at 0 to 5 ns .....	58
Figure 50.	Time gate with corresponding distance from antenna .....	59
Figure 51.	Ambient with time gate 25 – 40 ns, six meters from antenna .....	60
Figure 52.	RCS of a 0.22 by 0.22 metal plate with time gate for six meters (with background subtraction).....	61
Figure 53.	Comparison between plate on a wooden stand versus hanging from the ceiling, with time gate for six meters (with background subtraction) .....	62
Figure 54.	RCS of wire hang vertically from ceiling, with time gate for six meters (with background subtraction).....	62
Figure 55.	Comparison between three targets, with time gate on at six meters (with background subtraction).....	63
Figure 56.	A 0.22 by 0.22 meter plate five meters from the antenna.....	64
Figure 57.	Comparison plot for 0.22 by 0.22 meter plate at five and six meters (with background subtraction).....	65
Figure 58.	Wire hang from ceiling, five meters from the antenna .....	65
Figure 59.	Comparison of returns for a wire hung from the ceiling, at five and six meters (with background subtraction) .....	66
Figure 60.	Comparison plots between the plate and wire, with time gate for five meters (without background subtraction) .....	67
Figure 61.	Frequency averaged scattering plots for the plate and wire (without background subtraction).....	67
Figure 62.	Comparison between vertical wire and ambient, with time gate for five meters (without background subtraction) .....	68
Figure 63.	Horizontal wire placed one meter above the floor, five meters from the antenna .....	69
Figure 64.	Horizontal wire placed two meters above the floor, five meters from the antenna .....	69
Figure 65.	Comparison between vertical and horizontal wires at one meter height, with time gate for five meters (without background subtraction).....	70

Figure 66.	Comparison between vertical and horizontal wires on the floor, with time gate for five meters (without background subtraction).....	71
Figure 67.	Comparison between vertical and horizontal wires at two meter height, with time gate for five meters (without background subtraction).....	71
Figure 68.	Diagonal wire placed five meters from the antenna .....	72
Figure 69.	Comparison between vertical and diagonal wires, with time gate for five meters (without background subtraction) .....	73
Figure 70.	Vertical wire placed one meter right of main beam.....	74
Figure 71.	Vertical wire placed one meter left of main beam.....	74
Figure 72.	Comparison between ambient and vertical wire one meter to the right, with time gate for five meters (without background subtraction).....	75
Figure 73.	Comparison between ambient and vertical wire one meter to the left, with time gate for five meters (without background subtraction).....	75

THIS PAGE INTENTIONALLY LEFT BLANK

## LIST OF TABLES

Table 1.	Summary of low frequency tradeoffs (From [7]) .....	18
Table 2.	Summary of high frequency tradeoffs (From [7]) .....	18
Table 3.	Grazing angles vs. range (From [7]) .....	27
Table 4.	Summary of time gate with distance.....	59

THIS PAGE INTENTIONALLY LEFT BLANK



## **LIST OF ACRONYMS AND ABBREVIATIONS**

AWG	American Wire Gauge
CCD	Coherent Change Detection
CEM	Computational Electromagnetic
CFAR	Constant False Alarm Rate
CWIE	Command Wire-Improvised Explosive Device
EMI	Electromagnetic Induction
GPR	Ground Penetrating Radar
HMDS	Husky Mounted Detection System
HPBW	Half-Power Beamwidth
ICA	Independent Component Analysis
IED	Improvised Explosive Device
OCD	Optical Change Detection
PCA	Principle Component Analysis
PGF	Path Gain Factor
PPF	Pattern Propagation Factor
PRF	Pulse Repetition Frequency
RAM	Radar Absorbing Material
RCS	Radar Cross Section
SAR	Synthetic Aperture Radar
SCR	Signal-to-Clutter Ratio
SNR	Signal-to-Noise Ratio
UAV	Unmanned Air Vehicle

THIS PAGE INTENTIONALLY LEFT BLANK

## EXECUTIVE SUMMARY

Due to the recent success in jamming wireless improvised explosive devices (IEDs), the threat nowadays has shifted towards the use of buried command wires. The wire could be more than several hundred meters long and buried several inches below the ground surface. Over the years, two types of radar detection, the ground penetrating radar (GPR) and synthetic aperture radar (SAR) have been developed to counter the IED threat. However, the data collection process for both radars is slow and, hence, introduces a significant time delay before target information can be obtained.

The main focus of this thesis is to investigate the wire scattering behavior and clutter characteristics for the command wire sensor system. The first problem encountered was the transmit-receive leakage issue. The close proximity between the two horns causes some of the power to leak directly from the transmit horn to the receive horn. Further tests were conducted with various layers of absorber placed between the horns. The measurement results showed that inserting two pieces of absorber reduces the leakage by 12 dB. As a result, for the command wire measurements, two pieces of absorber were used to reduce the leakage.

Although the leakage problem has been resolved, the initial wire measurements with background subtraction showed very low scattering returns, approximately in the range of 1 dB for wires laid on the ground as well as wires hung vertically from the ceiling. This level is not large enough to be useful for a command wire sensor in a clutter environment. Hence, the next approach was to conduct a sensitivity measurement with a calibration target. After determining a plate's dimension so that its half-power beamwidth (HPBW) would cover both antennas, a 0.22 by 0.22 meter metallic plate was fabricated. The metal plate measurements showed rapidly (in frequency) fluctuating peaks in the range of 3 to -6 dB. The measurement of a 3.2 meter metal pole also demonstrated similar fluctuating characteristics. Even though background subtraction is used, the conditions change once the target is placed in the chamber. The fluctuations observed are

due to the multiple reflections within the anechoic chamber, and interactions of the target with the chamber side walls, floor and ceiling. Therefore, time gating is required to eliminate the multipath components.

After determining the time gating period that corresponds to the distance within the chamber, the wire scattering measurements showed significant improvements in terms of a higher return (approximately 10 dB). The next approach was to eliminate the effect of the pedestal to the measurement results. The wire was measured at five meters from the antenna with time gating and with the pedestal out of the time gating range. The results show an improved 30 dB return, hence proving that the pedestal does indeed lower the scattering returns of the target by at least 20 dB.

The next approach was to compare the measurements with and without background subtraction. Without background subtraction, the average plots showed a scattering difference of 17.1 dB between ambient and the wire, as well as a 21.6 dB between the wire and the plate. Measurements between different horizontal, vertical and diagonal wires were also presented. From the results, it is clear that the wire scattering return is the highest when the wire is aligned with the horn polarization. There will always be a component parallel to the wire if circular polarization is used in the sensor system.

In conclusion, several technical challenges with regards to the command wire sensor were addressed. The significant transmit-receive coupling was identified, and leakage reduction was resolved. Various wire scattering and clutter characteristics were illustrated with the measurements. The theoretical calculations were also validated with actual measurements. Last but not least, the measurements have demonstrated close-in clutter rejection by utilizing time gating.

## **ACKNOWLEDGMENTS**

I would like to express sincere thanks to my thesis advisor, Professor David C. Jenn, for his support, guidance, patience and time throughout the course of this thesis. He always answered all my questions patiently and assisted me with any problem that I had during the preparation of this thesis. I could not have completed this thesis without the assistance for Professor Jenn.

I would like to thank Professor Tri T. Ha, who is my second reader for this thesis. I would also like to express my appreciation to Mr. Robert Broadston for his assistance in helping me set up the anechoic chamber for all my measurements, as well as for his kind assistance in the use of the facilities at the microwave laboratory.

I am grateful for Singapore Technologies Kinetics for providing this opportunity to study at the Naval Postgraduate School.

Last but not least, I would like to thank my wife Cheryl for her encouragements and kind understanding throughout my course of study.

THIS PAGE INTENTIONALLY LEFT BLANK

# I. INTRODUCTION

## A. BACKGROUND

An improvised explosive device (IED), also known as a roadside bomb, is a homemade bomb built and deployed in ways other than in conventional military warfare. It may be constructed of conventional military explosives, attached to a detonating mechanism [1]. IEDs were used extensively in Afghanistan by insurgent groups, and IEDs have become the most common form of attack against NATO forces. In fact, IED attacks have been increasing consistently every year. IEDs have various triggering mechanisms, including remote control, infra-red or magnetic triggers, pressure-sensitive bars or trip wires, as shown in Figure 1. Many new technologies have been developed that are capable of detecting, disrupting or disabling wirelessly triggered IEDs. For example, jammers are designed to create a “bubble” of protection around troops operating in combat situations. Many combat vehicles are now equipped with radio frequency jamming devices, which can disrupt the cell phone signals often used to trigger the IEDs.



Figure 1. The IED threat (From [2])

Due to the recent success in jamming wireless IEDs, the threat nowadays has shifted towards the use of buried command wires. A command wire-improvised explosive device (CWIED) uses an electrical firing cable that allows the user to have complete control over the device [1]. The bomber uses a switch wired to the IED to initiate the detonation. A command wire is a hair-thin, bare copper strand that only the sharpest eye can see. The wire can be more than several hundred meters long and buried several inches below the ground surface, as shown in Figure 2. In addition, it is very difficult to spot the wires visually, especially onboard a vehicle travelling at more than 20 mph.



Figure 2. Soldiers trying to uncover a command wire (From [3])

Over the years, many types of radar have been developed for buried wire detection. A key technology in seeking IEDs below ground has been the use of ground penetrating radar (GPR). GPR uses radar pulses to form images of objects below the surface. This nondestructive method uses electromagnetic radiation in the microwave band of the radio spectrum and detects the reflected signals from subsurface structures. GPR can be used in a variety of media, including rock, soil, ice, fresh water, pavements and structures. It can detect objects, changes in material, voids and cracks [4]. However, subsurface radar must operate close to the surface, making it vulnerable to the IEDs that it is searching for. Also, the data collection process is slow, so the results are not



available in real time. Another type of radar system, the synthetic aperture radar (SAR), has huge potential for wire detection. SAR provides high-resolution imagery from airborne or space-borne platforms, coupling the long-range propagation characteristics of radar signal and digital electronics [5]. SAR works by repeatedly illuminating a target area with pulses of radio waves at wavelengths anywhere from a meter down to millimeters. The many echo waveforms received successively at the different antenna positions are coherently detected, stored and then processed together to resolve elements in an image of the target region [6]. As in the case of GPR, data collection and processing introduces a significant time delay before target information and image are obtained.

## **B. OBJECTIVE**

A capability to immediately detect the presence of a command wire would be of great value to the troops on the ground. In FY 2009, NPS was tasked to investigate a command wire sensor that is portable and can operate in real-time [7]. The outcome of that research was that equations for the ground clutter and wire scattered signal were derived, and software simulations were performed to estimate the signal-to-clutter ratio (SCR) for a range of sensor parameters. Due to contradictory published data, there was more than 20 dB of uncertainty presented in the combined variations in models for wire scattering and clutter return. Hence, there is a need to accurately define the wire scattering and ground clutter properties before the sensor system can be evaluated with confidence.

The work in this thesis concentrates on investigating the wire scattering behavior and clutter characteristics. Computational electromagnetic (CEM) software was used to compute command wire scattering, and measurements were performed in the NPS anechoic chamber located in Spanagel Hall, Room 604. A reconfiguration of the chamber instrumentation was necessary to perform the measurements. These measurements were then used to evaluate previous simulation results.

## **C. THESIS OUTLINE**

This thesis is broken into five chapters. The current technologies used for IED detection are introduced in Chapter I. A review of previous work done, background on existing IED detection systems, as well as the challenges in designing a command wire sensor, are discussed in Chapter II. The theory behind wire scattering, clutter modeling, detection contours, time gating and false alarms are described in Chapter III. In Chapter IV, the measurement results are presented. The findings of this research, conclusions and recommendations for future research are summarized in Chapter V.

## **II. REVIEW OF PREVIOUS WORK**

A review of existing IED detection systems, focusing on two key detection systems, the ground penetrating radar and synthetic aperture radar, are discussed in this chapter. In addition, the key challenges in designing a command wire sensor are also discussed.

### **A. EXISTING DETECTION SYSTEMS**

Much work has been done on systems that can detect IEDs at standoff distances that are far enough to survive if the IED blows up. A few years ago, troops in Iraq were reportedly using a system called PING [8]. This system emits microwave signals that penetrated building walls. If the signals encountered an IED with large amounts of metal, those signals would be altered in a way that could be detected with reasonable consistency. Some of these standoff systems depend on radically new technologies, such as terahertz-frequency and millimeter-wave radiation, or on radical applications of existing technology. Several have already been deployed, with limited success. The existing technologies include visible light lasers, ground-penetrating radar, synthetic-aperture radar, thermal imaging, magnetic resonance, and electronic “sniffers” that can detect in the air infinitesimal concentrations of molecules from explosives. A sniffer called Fido is currently being used in Iraq and Afghanistan. There is a handheld version and also one attached to a small robot. Fido uses a polymer-based technology to achieve faster explosive detection results. It helps users to pinpoint people involved in the construction, transportation and deployment of explosive devices. Although the Fido system works well, it does so only for a limited number of explosives, and the only standoff capability you get is from the robot.

In June 2010, the U.S. Army purchased another 76 HMDS (Husky Mounted Detection System) IED detectors [9]. HMDS is actually a ground penetrating radar (VISOR 2500) that can see what is under the road ahead. One of the enduring frustrations with IEDs in Afghanistan is that often components are nonmetallic and nonmagnetic, making them difficult to detect using conventional methods. The GPR allows soldiers to

detect threats through the ground that metal detectors would not pick up, enabling combat engineer units to quickly and regularly check heavily used roads for IEDs. An HMDS can scan a road at speeds of up to 12 kilometers an hour. The stored scan data is used to improve the accuracy of the analysis and prediction software. As the system is not 100 percent accurate, there is an ongoing process to gather more past data into the system in order to improve its accuracy. The HMDS vehicle with GPR is shown in Figure 3.



Figure 3. Husky mine detection vehicle with ground penetrating radar (From [10])

## **B. GROUND PENETRATING RADAR**

Buried landmines and IED detection using electromagnetic induction (EMI) techniques is well established, and a range of metal detectors is commercially available [4]. Recent developments using dual sensor technology combining EMI and ground penetrating radar (GPR) have enabled improved discrimination against small metal fragments to be demonstrated in live minefields.

### **1. GPR for Landmine Detection**

GPR is an electromagnetic technique which is used to measure the depth and position of landmines buried within the ground or dielectric material [4]. For landmine

detection, it is important that the radiated power is lower than that required to initiate the detonating fuses. The power loss through the soil is often measured as a propagation loss in decibels per meter and is dependent on the conductivity of the soil and the frequency of operation. Soil is a lossy dielectric whose relative dielectric constant depends mainly upon the water content. Typically, the relative dielectric constant of the soil varies from three in dry sand to greater than 16 in wet and waterlogged soils. GPR must be operated with the antenna very close to the ground surface so that the energy transfer is predominantly either induction or quasi-stationary (the near field). Due to the extremely high levels of clutter at short ranges, the signal-to-noise ratio (SNR) poses a major technical challenge in GPR design.

GPR system design can be classified into two categories. Systems that transmit an impulse and receive and process the reflected signal from the landmine using a sampling receiver can be considered to operate in the time domain. Systems that transmit individual frequencies in a sequential manner or as a swept frequency and receive the reflected signal from the landmine using a frequency conversion receiver can be considered to operate in the frequency domain. The GPR image of a landmine is very different from its optical image due to the similarity in dimensions between the wavelengths of the illuminating radiation to the landmine. As a result, the GPR image is a lower definition image that is highly dependent on the propagation characteristics of the ground. The beam pattern of the antenna is widely spread in the dielectric, and this degrades the spatial resolution of the image. Refraction and anisotropic characteristics of the ground may also distort the image.

There is an extensive literature on radar methods for landmine detection, and a variety of sophisticated modeling and processing methods have been applied to the problem. However, the nature of operation in real soils coupled with the extreme harsh terrain has meant that few of these techniques have proved robust enough when moved from the laboratory to the field.

## 2. Attenuation

Electromagnetic waves propagating through soil incur an attenuation loss in dB given by [4]

$$L_a = 8.686(2)(R)(2\pi f) \sqrt{\left( \frac{\mu_0 \mu_r \epsilon_0 \epsilon_r}{2} \left( \sqrt{1 + \tan^2 \delta} \right) - 1 \right)} \quad (1)$$

where  $f$  is the frequency in Hz,  $\tan \delta$  is the loss tangent of the soil,  $\epsilon_r$  is the relative permittivity of the soil,  $\epsilon_0$  is the permittivity of free space,  $\mu_r$  is the relative magnetic susceptibility of the soil,  $\mu_0$  is the permeability of free space, and  $R$  is the range in meters.

The graph shown in Figure 4 is the two-way attenuation loss in decibels per meter versus frequency for a material with a relative dielectric constant of nine and loss tangents of 0.1 to 0.9 in steps on 0.3 [4]. As the frequency increases from 1 GHz to 5 GHz, the attenuation loss for a soil with a loss tangent of 0.3 increases from 20 to 100 dB.

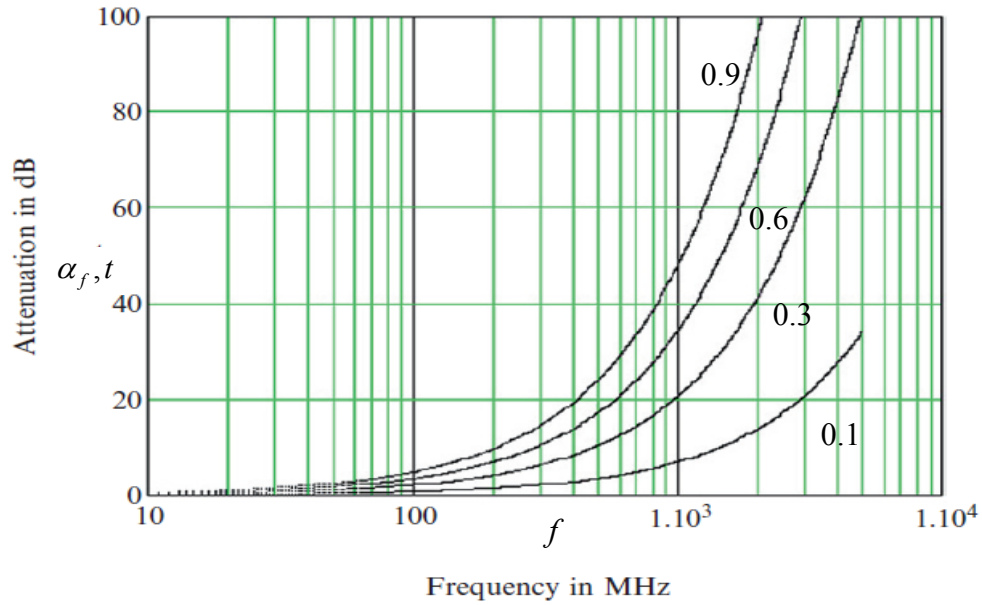


Figure 4. Propagation losses plotted against frequency for several values of  $\tan \delta$  (After [4])

The effect on the spectrum of a typical radar pulse is shown in Figure 5. The peak of the spectrum is shifted to lower frequencies, and the higher frequencies are considerably reduced.

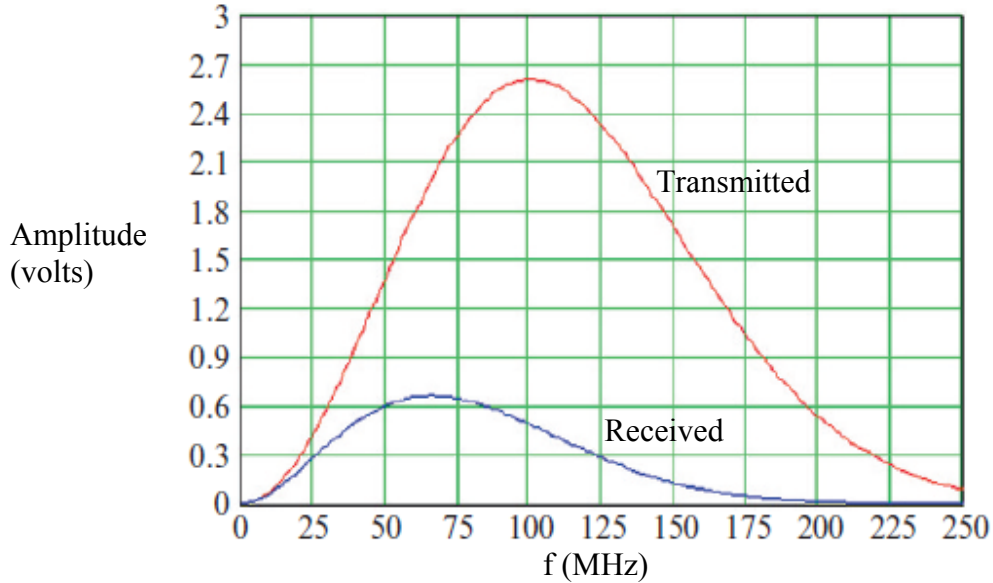


Figure 5. Spectrum of transmitted and received signals after passing through lossy ground (After [4])

### 3. Coupling Energy into the Ground

Buried mines pose a difficult detection problem for radars, and their performance is strongly influenced by the ground conditions [4]. For a close-in operation, the efficiency of the coupling process is high, but this is not the case for standoff radar systems. The reason for this is because there are lossy materials, and complex angles of refraction may occur.

Brewster's angle (also known as the polarization angle) is the angle of incidence at which a wave with parallel polarization is perfectly transmitted through a dielectric surface with no reflection [11]. Parallel polarization occurs when the electric field vector lies in a plane defined by the surface normal and the incident propagation vector [12]. For small grazing angles ( $\psi = 90 - \theta_i \approx 0$ ) parallel polarization is very nearly vertical relative

to the ground. Therefore, it is also referred to as vertical polarization. When an unpolarized wave is incident at the Brewster angle, the wave that is reflected from the surface is perpendicularly polarized, as shown in Figure 6.

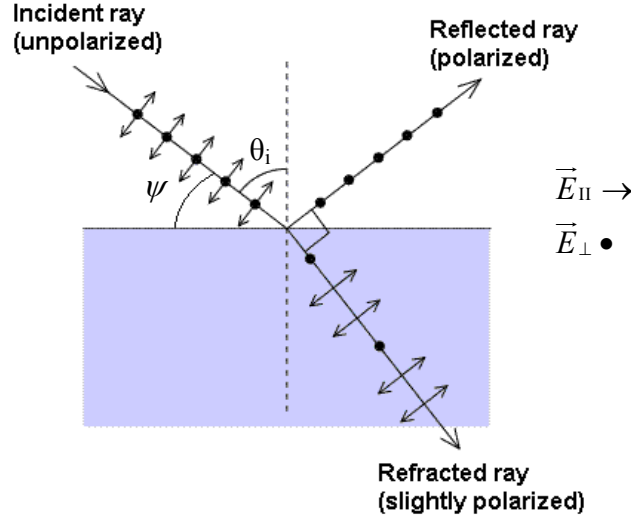


Figure 6. Parallel polarized wave incident on an interface at the Brewster angle (After [11])

With vertical polarization at incidence angles less than the Brewster angle, transmission losses at the air/ground interface are relatively small [4]. However, at a larger incidence angle than the Brewster angle, the losses increase more rapidly. As a result, in order to maximize the operating range, the radar should be mounted as high off the ground as possible. Hence, for a given height, the performance of the radar is affected by the relative dielectric constant of the ground.

The effective cross-section of all landmines decreases when they are buried in the ground. As a result, a metal landmine SCR is expected to be degraded on burial by approximately 10 dB. As for plastic mines, the cross-section is reduced by a larger factor. This is due to the reduced dielectric contrast between the plastic and the surrounding soil. Hence, plastic mines are more readily detected in wet sandy soils as compared to dry conditions. On the other hand, plastic mines, when designed with air voids, are subjected to substantially smaller burial losses in dry sand. The radar system must have at least a 20 dB SCR to detect buried landmines in all weather conditions. Thus, in order to detect



buried plastic landmines with air voids, the signal-to-clutter ratio for surface laid metal landmines must be better than 12 dB for dry conditions and 18 dB for wet conditions.

#### **4. Clutter**

A major difficulty for operation of GPR systems is the presence of clutter within or on the surface of the material or in the side and back lobes of the antenna [4]. Clutter is defined as sources of unwanted reflections that occur within the effective bandwidth and search window of the radar and are present as spatially coherent reflectors. Clutter can completely obscure the buried landmine, and a proper understanding of its source and impact on the radar is essential. Abrupt discontinuities can also cause multiple reflections which become superimposed on later arriving reflected energy. Such “interference” is extremely difficult to remove.

#### **5. Vehicle Based Radar Systems**

Vehicle based systems have been developed that use arrays of antennas to generate three-dimensional (3-D) data [4]. The data is then processed to provide a rolling map of detections. In general, vehicle based systems focus on anti-tank landmines because it is difficult to achieve adequate cross range resolution with realistic budgets. Options for signal and image processing include image inversion and synthetic aperture techniques for image enhancement principle component analysis (PCA), independent component analysis (ICA) techniques, and hidden Markov models. Most GPR systems achieve optimum performance in terms of range when the antennas are operated in close proximity to the ground. As the antenna-to-ground spacing increases, the antenna radiation pattern results in reduction of the received signal from small landmines and increased vulnerability to clutter from free space sources.

### **C. SYNTHETIC APERTURE RADAR**

A synthetic aperture radar (SAR) is a coherent airborne or spaceborne side-looking radar system which utilizes the flight path of the platform to simulate an extremely large antenna or aperture electronically so as to generate high-resolution

remote sensing imagery [13]. Over time, individual transmit/receive dwells are completed with the data from each dwell stored electronically. The signal processing uses the magnitude and phase of the received signals over successive pulses to form a synthetic aperture. After a given number of cycles, the stored data is recombined to create a high resolution image of the target area.

## **1. Applications**

SAR produces a high-resolution image of a scene of the earth's surface in both range and cross-range [14]. It can produce images of scenes at long range and in adverse weather, which is not possible with infrared or optical sensors. SAR produces a high resolution image of a scene by synthesizing in its processor the equivalent of a large antenna to obtain good resolution in the cross-range direction. High resolution in the range direction is obtained by either a short pulse or pulse compression. A good SAR might have a resolution in range and cross-range of one meter, but it can be much less if desired.

A conventional SAR is normally designed to image stationary objects and does not accurately image moving targets. Moving targets can be seriously distorted and displaced from their true location. Thus, SAR is restricted to the recognition of stationary objects. One application of SAR is its military use for airborne surveillance of the battlefield and for imaging of fixed targets. Moving targets can be detected with a SAR if they have a Doppler frequency shift greater than the spectral bandwidth of the stationary ground clutter echo. Clutter in this case is the desired signal for a SAR. However, this technique is limited since it needs a pulse repetition frequency (PRF) high enough to avoid Doppler foldover of echo signals. A high PRF, on the other hand, may give rise to range ambiguities. Moreover, this method for extracting moving targets with a SAR may not be able to detect moving targets that have low radial velocity.

A more suitable solution is to use a UAV loitering overhead, equipped with ground surveillance systems to monitor the area ahead of a convoy to detect IEDs lying ahead, as shown in Figure 7. Synthetic aperture radar can also be employed by "sweeping" roadsides from long distance and detecting changes in the terrain, which

could indicate IED locations. To better coordinate between the UAV and the convoy, the UAV or its sensor has to be controlled from the moving vehicles, providing a continuous feed of video imagery while on the move.



Figure 7. SAR mounted on the Predator UAV (From [16])

Scientists working for the United States Navy have used a technique that involves an airborne polarimetric SAR on overhead platforms to remotely identify sites within a search area where IEDs have been hidden [15]. The radar-based IED detection method offers warfighters several potential advantages, such as improved levels of identification and, as a result, more thorough associated intelligence data. By drawing on a number of polarizations and viewing angles, it can display information down to a single pixel level and can render scenes with an astonishing amount of detail. New detection techniques will lead to enhanced remote sensing capabilities with immediate application to asymmetric operations and battle space awareness in addition to intelligence, surveillance, reconnaissance and targeting applications.

## **2. Change Detection**

IED detection remains a crucial part of modern warfare. In recent years, the U.S. military has put multiple new detection technologies into service to counter the IED threat. There are different types of change detection which have been successfully utilized with great success. Examples of proven change detection capabilities are optical change detection (OCD) and coherent change detection (CCD) [16]. Change detection utilizes imagery collected from manned and unmanned air assets to digitally overlay,

compare and analyze changes in the pixels of time-separated images to exploit any man-made disturbance such as new or moved objects, footprints, tire tracks or even faintly disturbed earth.

The main difference between these two types of imagery change detection is that OCD exploits high resolution photographic imagery while SAR CCD exploits synthetic aperture radar imagery. With reference to Figure 8, the SAR CCD example provides insight to imagery processing and exploitation. The referenced black areas represent disturbances assumed to be foot traffic, resulting in pixel changes between the two separated images. The white areas represent zero disturbance or areas void of activity.

The successful employment of change detection on the battlefield has made it the capability of choice for many other intelligence, surveillance and reconnaissance missions. These missions include detection of enemy activity along vehicle routes/remote fields/pastures/river banks, coalition base security perimeters, concealed enemy traffic routes and pattern of life analysis for potential areas of interest. The primary advantage of OCD and SAR CCD is the ability to exploit all enemy efforts of concealment. In other words, more deliberate concealment results in more significant disturbances identified through change detection.

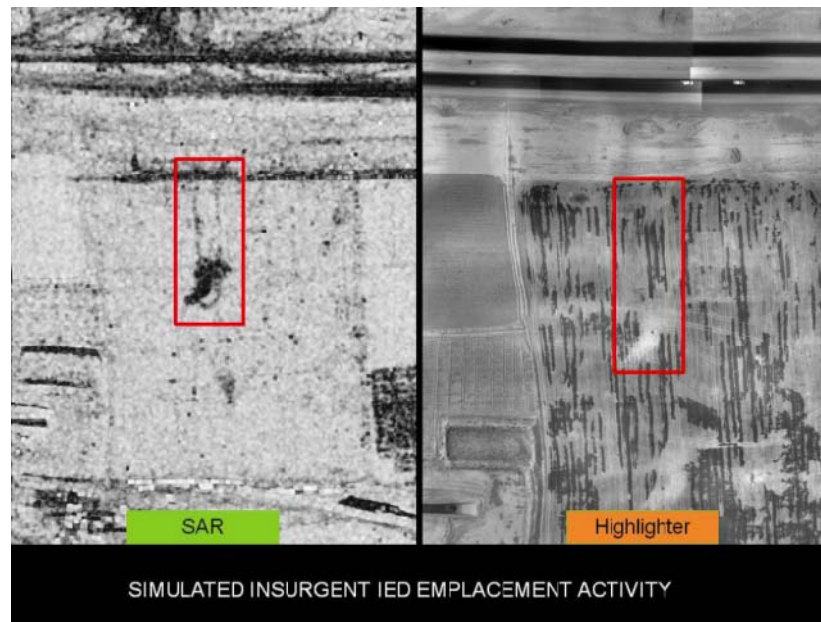


Figure 8. Example of SAR CCD (From [16])

#### **D. COMMAND WIRE SENSOR SYSTEM CHALLENGES**

In 2009, NPS was tasked to investigate a command wire sensor that is portable and can operate real-time [7]. The concept is illustrated in Figure 9. This section presents a synopsis of the study's final report.

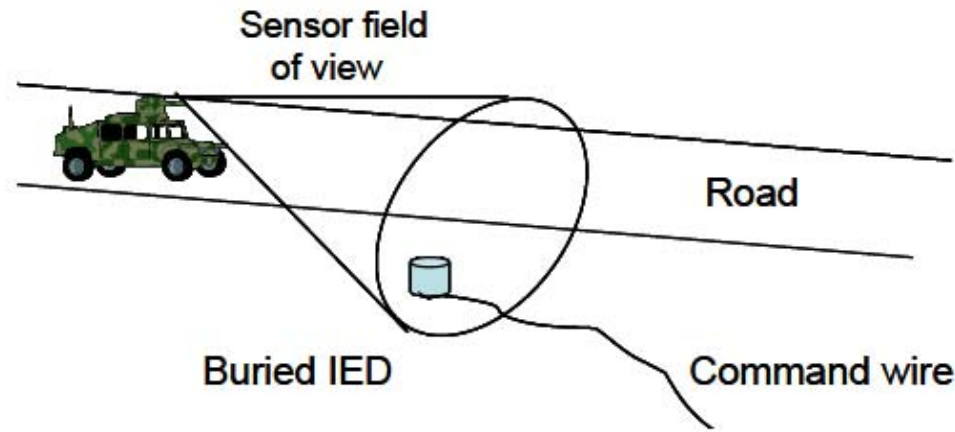


Figure 9. Vehicle mounted command wire sensor (From [7])

The desirable operating conditions for the command wire sensor are as follows:

1. Safe detection ranges, minimum range at 100 meters.
2. High probability of detection, low probability of false alarm, high search rate.
3. Able to detect over a wide range of wire aspect angles.
4. Find wires buried in a wide range of ground materials and ground cover.
5. Minimize cost, complexity and size.

The command wire sensor concept is similar to a monostatic radar. A monostatic radar is a conventional radar in which the transmitter and receiver are at the same location and share the same antenna. For this application, the main objective of the sensor is to detect the presence a wire. Therefore, it is not necessary to have a high resolution image. As a result, data processing is reduced significantly. The major challenge of the

command wire sensor is to detect the wire in clutter and achieve a high probability of detection without large number of false alarms.

Compared to a conventional radar system, the command wire sensor system will be operating under significantly different conditions. As a result, many of the standard radar assumptions do not apply. Several important considerations are:

1. A command wire at close range is not a point target.
2. A command wire is a linear (two-dimensional) scatterer and responds only to waves polarized along the wire axis.
3. The sensor is in the near-scattered field of the wire.
4. Due to the antenna's close proximity to the target and ground, plane wave propagation cannot be assumed.
5. The ground clutter characteristic at low grazing angle is an area that has not been investigated.

## **1. Wire Scattering**

The general sensor-wire geometry is shown in Figure 10. Although there will be quite a wide variety of command wire geometries encountered, it is very likely that there will be a long straight section somewhere along the path. A long linear wire has a significant scattering cross-section for waves that are polarized along its axis. However, wire scattering is expected to be small for cross-polarized waves or when the wire is viewed end on. Therefore, in order to maximize the axial field component, circular polarization is required.

A travelling wave can be excited when long wires are illuminated with vertical polarization at low grazing angles, resulting in a high electromagnetic scattering cross-section. The fact that the travelling waves can be excited at relatively small angles from the wire axis makes it ideal to deploy a man portable or vehicle mounted antenna that transmits a signal to excite the travelling wave. In addition, the travelling wave can also be induced by the vertical component of the incident field. Therefore, even if the antenna

height is only a few meters, it can still be excited at end-on aspect angles. Furthermore, operating in the near-scattered field of the wire broadens scattering lobes and may improve the probability of intercept.

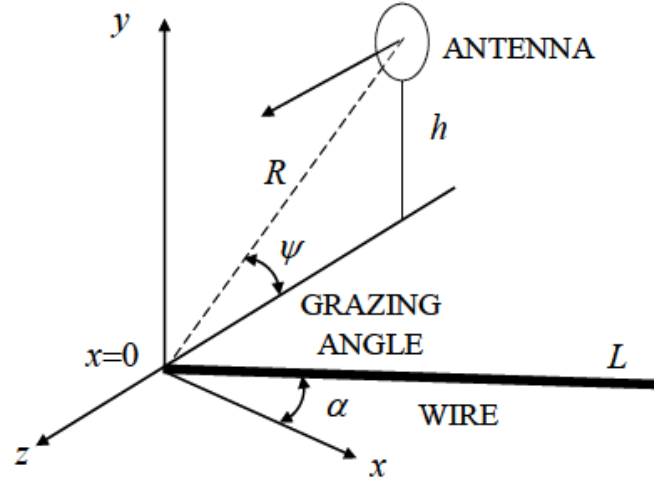


Figure 10. General sensor-wire geometry (From [7])

## 2. Propagation and Frequency Considerations

Several frequency and propagation tradeoffs need to be considered for the command wire sensor design [7]. Lower frequencies travel more efficiently as ground waves. This is because they are more strongly diffracted around obstacles due to their long wavelengths. Hence, at lower frequencies, surface waves can be coupled from the antenna to the ground-air interface. The surface wave field extends into the ground and does not suffer the loss of plane wave reflection. As a result, the scattering from buried wires is enhanced. In addition, polarization blindness is mitigated due to surface wave propagation. As this mode of propagation is not excited at higher elevation angles, it is often not seen by a UAV or helicopter based radar. The summary of low frequency tradeoffs is shown in Table 1.

At higher frequencies, the terrain features are more critical. Surface roughness may increase clutter if specular backscattering occurs. The rough terrain surface may also introduce shadowing, blockage, and multiple reflections if the deviations are significant

compared to the wavelength. In general, higher frequencies allow smaller, lighter-weight components as compared to lower frequencies, resulting in smaller hardware components. However, the antenna size is less of a problem if a low gain antenna is used even if a low frequency is used. The advantages and disadvantages of utilizing high frequencies are summarized in Table 2.

Table 1. Summary of low frequency tradeoffs (From [7])

<b>Low Operating Frequency</b>	
<b>Advantages</b>	Surface and travelling waves at low grazing angles.
	Low attenuation when propagating through the ground.
	Near-field wire scattering, broader scattering lobes.
	Surface roughness not normally a problem.
<b>Disadvantages</b>	Requires a large antenna (~ 3 feet)
	Large antenna half-power beamwidth increases clutter.

Table 2. Summary of high frequency tradeoffs (From [7])

<b>High Operating Frequency</b>	
<b>Advantages</b>	Small antenna beamwidth yields less clutter.
	Smaller hardware components.
<b>Disadvantages</b>	Narrow wire scattering lobes means scattered signal is more aspect dependent (lower probability of intercept).
	Small antenna beamwidth also means more search time and less wire illuminated.
	Larger ground attenuation.
	Surface roughness (shadowing and blockage of wire).



According to [17], we know that when the wire radius is much less than a wavelength (i.e., frequencies below 1 GHz), the current density induced on the wire is nearly independent of radius. Therefore, decreasing the radar frequency does not significantly diminish the wire scattering for a fixed length; although, it does improve ground penetration.

### **3. Clutter Characteristics**

The major contributing factor of the command wire detection depends largely on the signal-to-clutter ratio. Increasing the transmitter power does not make detection any easier, as both the signal and clutter are increased in the same proportion when the transmitter power is increased. Thus, there is no improvement in the SCR. In order to improve SCR for a fixed wire return, it is more effective to reduce the clutter power. The clutter power is controlled by ground return at short ranges. By utilizing time gating, much of the close-in clutter return can be rejected. Clutter rejection can also be achieved using circular polarization. Since the ground reflections have the opposite sense, ground reflections will not be received by the antenna; hence, polarization mismatch results in clutter rejection.

### **E. SUMMARY**

In this chapter, various IED detection systems were discussed, highlighting both the GPR and SAR detection techniques and applications. The command wire sensor design challenges with respect to wire scattering, frequency considerations and clutter characteristics were elaborated. Various wave propagation and clutter modeling theory are the focus of the next chapter.

THIS PAGE INTENTIONALLY LEFT BLANK

### III. THEORY

In this chapter, various wire scattering theories, including multipath, are discussed. Clutter modeling and time gating theory is also introduced. Probabilities of detection and false alarms are also addressed.

#### A. WIRE SCATTERING

##### 1. Travelling Waves

A travelling wave is one type of surface wave [18]. The surface impedance supports a transmission line mode. The incident wave is captured by the surface or wire and transformed to a wave guided along the interface.

If the wire is finite (i.e., has an end) then some of the travelling wave will be radiated off the edge in the forward direction and some reflected, as shown in Figure 11. The reflected wave radiates as it travels in the reverse direction. This effect is a maximum at an edge incidence angle of approximately [18]

$$\theta \approx 49.35^\circ \sqrt{\frac{\lambda}{L}} \quad (2)$$

where  $\lambda$  is the wavelength and  $L$  is the wire length.

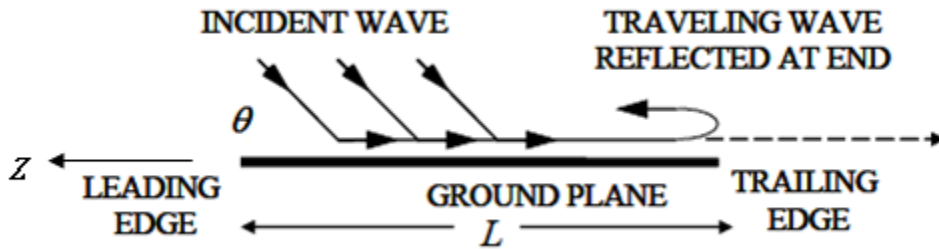


Figure 11. Travelling waves reflection (From [18])

From [14], an experiment was conducted that illustrates the radar cross section (RCS) characteristics of a long, thin wire. The wire is  $16\lambda$  long and  $0.01\lambda$  in diameter.

When viewed from the broadside ( $\theta = 90^\circ$ ), the RCS is relatively large. As the viewing angle departs from  $90^\circ$ , the RCS decreases rapidly. On the other hand, as the viewing angle decreases, an angle is reached where the backscatter levels off and then increases. This is due to a surface travelling wave. Another experiment was done with a long thin rod. The incident electromagnetic wave couples onto the wire which then travels the length of the rod and reflects from the discontinuity at the far end. The travelling wave is launched when the incident electric field is polarized in the plane of incidence defined by the surface normal and direction of incidence. A surface travelling wave is not excited if there is no electric field component in the plane of incidence. The effect of the travelling wave is prominent when the grazing angle is small and when there is a discontinuity at the far end of the body that reflects the travelling wave back to the radar. The travelling wave portion of the echo is reduced if the surface is made of resistive material, which causes attenuation as the waves travels down the surface and back.

## 2. Scattering by a Straight Thin Wire

Travelling wave energy can play a significant role in the overall scattered field of a straight wire [19]. The expressions for each scattering mechanism on a straight thin wire are cast in the form of four basic electromagnetic wave components: diffraction, attachment, launch and reflection. Each of the scattering mechanisms are combined to obtain the total scattered field for a straight thin wire.

Consider a wire of length  $L$  and radius  $a$ , centered on the  $z$ -axis, as shown in Figure 12. The scattering paths for a straight wire are depicted in Figure 13.

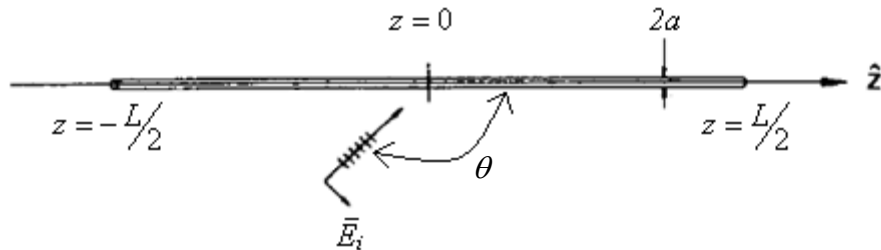


Figure 12. Geometry of straight wire (After [19])

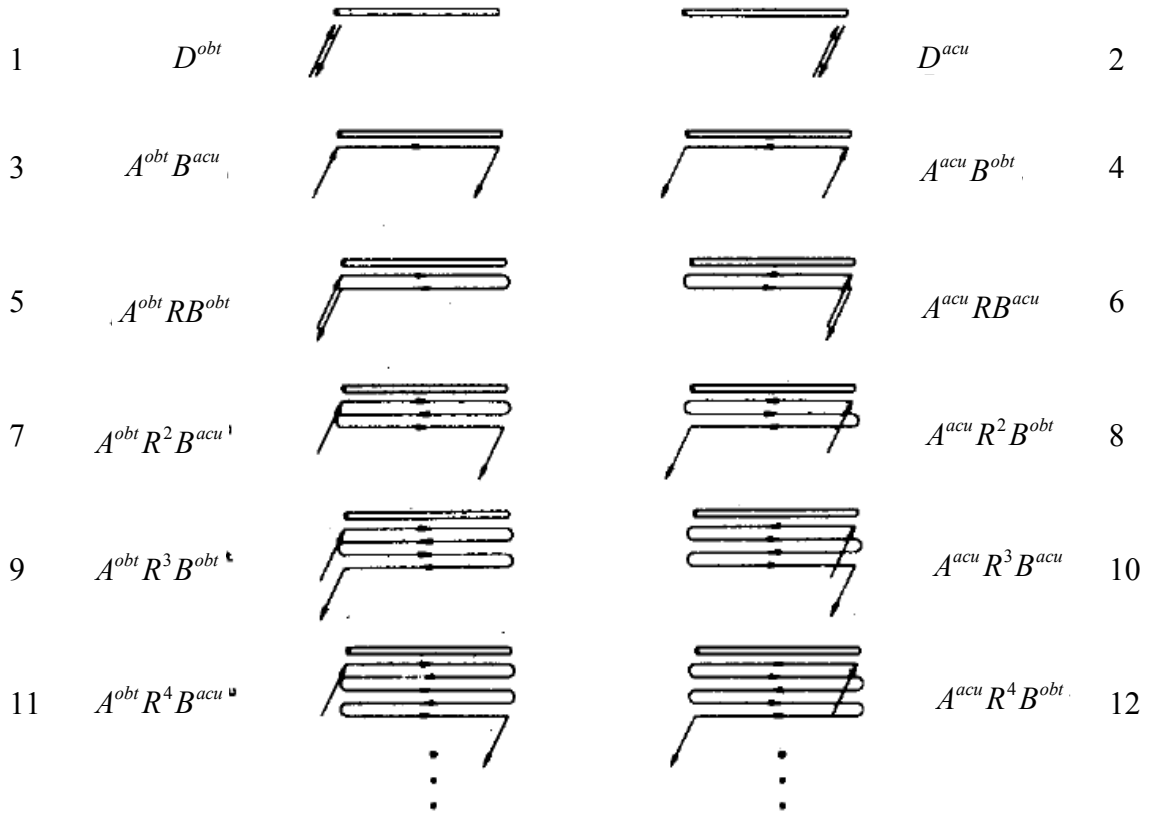


Figure 13. Scattering contributions for a straight wire (After [19])

The scattering mechanisms from a high frequency viewpoint for backscatter of an incident plane wave at an angle  $\theta$  upon a wire with the electric field in the plane of incidence, where the  $e^{j\omega t}$  time dependence is assumed and suppressed, are shown. The total scattering equation is approximated as:

$$\begin{aligned} \text{Total Scattering} = & D^{obt} e^{jkL \cos \theta} + D^{acu} e^{-jkL \cos \theta} + \frac{e^{-jkL}}{[1 - R^2 e^{-jk2L}]} \{ A^{obt} B^{obt} R e^{jkL(\cos \theta - 1)} \\ & + A^{acu} B^{acu} R e^{-jkL(\cos \theta + 1)} + A^{obt} B^{acu} + A^{acu} B^{obt} \} \end{aligned} \quad (3)$$

where  $A$  is the wave attachment coefficient,  $B$  is the wave launch coefficient,  $k$  is  $2\pi/\lambda$  and  $R$  is the wave reflection coefficient. The superscript “obt” refers to the obtuse angle between the wave and the wire, and “acu” refers to the acute angle between the wave and the wire.

In [19], the scattering as a function of angle and as a function of frequency is compared to the method of moments solution. The results showed excellent agreement between the method of moments results and the approximate solution, even to within a few degrees of grazing incidence. When transformed into the time domain, each term represents a distinct physical mechanism, as labeled in Figure 14.

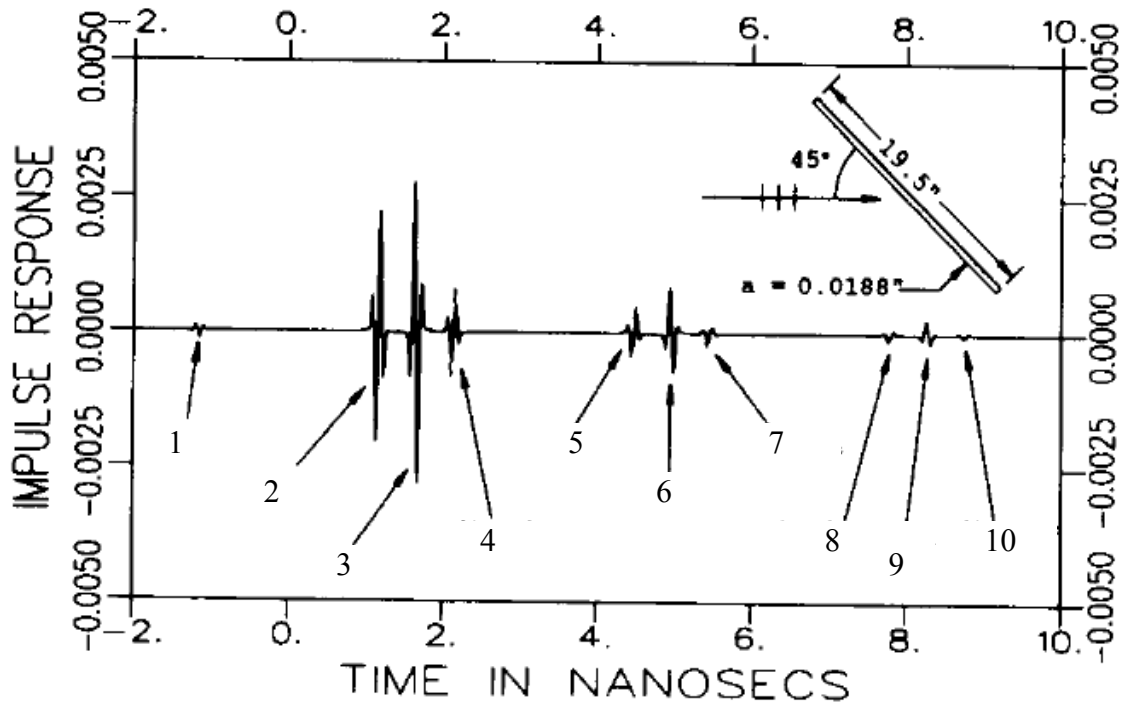


Figure 14. Band limited impulse response for a wire at  $\theta = 45^\circ$  (After [19])

Most of the existing work is focused on detecting wires as a point target, which means that the entire wire is in the far-field. However, wire detection for the command wire sensor may be extended beyond the main beam. It is possible that only part of the wire will be in the antenna half-power beamwidth. In addition, many of the references were looking at plane wave scattering from infinitely long wires, which is unlike the wire scattering model that the command wire sensor is detecting. Therefore, simulations and measurements are necessary to further examine the wire scattering characteristics for a command wire sensor.

### 3. Multipath

When both a transmitter and receiver are operating near the surface of the earth, multipath (multiple reflections) can cause fading of the signal [20]. These mirror-like reflections that obey Snell's law are called specular reflections.

The reflection coefficient is defined as  $\Gamma = |\Gamma|e^{j\phi_\Gamma}$ . For low grazing angles,  $\psi \approx 0$ , and the approximation  $\Gamma \approx -1$  is valid for both horizontal and vertical polarizations. The path difference can be termed as  $\Delta R = (R_1 + R_2) - R_0$ . If  $d \gg h_t, h_r$ , then the total field at the receiver is approximately

$$\begin{aligned} |E_{tot}| &= \underbrace{E_{ref}}_{\text{REFLECTED}} + \underbrace{E_{dir}}_{\text{DIRECT}} \\ &\sim \sqrt{G_t(\theta_A)G_r(\theta_C)} \frac{e^{-jkR_0}}{4\pi R_0} \underbrace{\left[1 + \Gamma e^{-jk\Delta R}\right]}_F. \end{aligned} \quad (4)$$

where  $G_t$  and  $G_r$  are the transmit and receive antenna gains, and gain  $F$  is the path-gain factor (PGF) or pattern-propagation factor (PPF). The symbol  $F$  relates the total field at the receiver to that of free space and takes on values  $0 \leq F \leq 2$ . If  $F = 0$ , the direct and reflected rays cancel each other, causing a destructive interference. If  $F = 2$ , the two waves add, resulting in constructive interference. If the transmitter and receiver are at the same height, close to the ground, and the antennas are pointed at each other, the PPF can be simplified to

$$|F| = |1 + \Gamma e^{-jk\Delta R}|. \quad (5)$$

### B. CLUTTER MODELING

Clutter may be defined as any unwanted radar echo [14]. It implies that these unwanted echoes “clutter” the radar and make difficult the detection of wanted targets. Clutter is generally distributed in spatial extent in that it is much larger in physical size than the radar resolution cell. When clutter echoes are sufficiently intense and extensive, they can limit the sensitivity of a radar receiver and limit range performance. The backscatter echoes from land can degrade the performance of many types of radar. Large

clutter echoes can mask echoes from desired targets and limit radar capability. When clutter is much larger than receiver noise, the optimum radar waveform and signal processing can be quite different from that employed when only receiver noise is the dominant limitation on sensitivity.

Echoes from land or sea are examples of surface clutter. The magnitude of the echo from distributed surface clutter is proportional to the area illuminated. Due to its distributed nature, the measure of the backscattering echo from such clutter is generally given in terms of a radar-cross-section density. The clutter cross section per unit area is independent of the illuminated area and is denoted by the symbol  $\sigma^0$ . For surface clutter, a cross section per unit area is defined as

$$\sigma^0 = \frac{\sigma_c}{A_c} . \quad (6)$$

where  $\sigma_c$  is the radar cross-section of the clutter occupying an area  $A_c$ . The clutter cross-section  $\sigma^0$  is a dimensionless quantity and is often expressed in decibels with a reference value of one  $\text{m}^2/\text{m}^2$ .

### 1. Surface-clutter Radar Equation

The radar equation describing the detection of a target in surface clutter is different from the standard radar equation. Consider the geometry in Figure 15 which depicts a radar illuminating a buried wire.

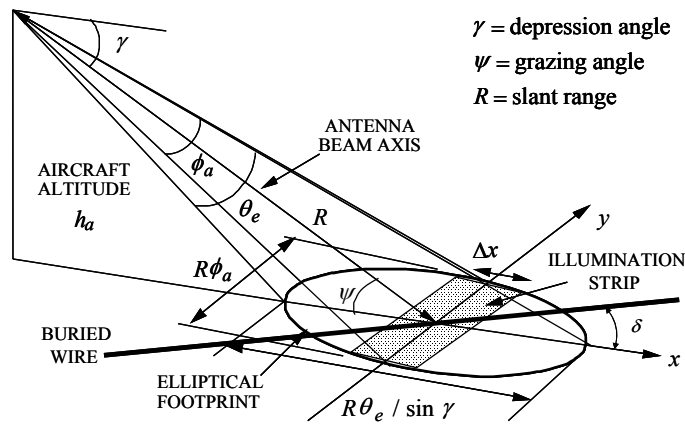


Figure 15. Antenna beam geometry (From [7])



In Figure 15,  $\gamma$  is the depression angle,  $\psi$  is the grazing angle (beam center to ground),  $R$  is the slant range,  $\theta_e$  is the elevation half power beamwidth,  $\phi_a$  is the azimuth half power beamwidth, and  $\delta$  is the wire angle from  $x$ -axis.

For the command wire sensor mounted on top of a vehicle, the antenna height is around 3 m. This low antenna height, along with the desire to see wires as far as possible, results in small grazing angles. The ranges and corresponding grazing angles are shown in Table 3. Note that the grazing angle is extremely small when looking out to a range of 200 m.

A small grazing angle usually implies that the extent of the resolution cell in the range dimension is determined by the radar pulse width  $\tau$  rather than the elevation beamwidth. The width of the cell in the cross-range dimension is determined by the azimuth beamwidth and the range  $R$ .

Table 3. Grazing angles vs. range (From [7])

$\psi$ (deg)	$\theta$ (deg)	$R$ (m)
10	80	17
5	85	34
2	88	86
1	89	172

From the radar range equation [14], the received echo power  $P_r$  is

$$P_r = \frac{P_t G A_e \sigma L_s}{(4\pi)^2 R^4} \quad (7)$$

where  $P_t$  is the transmitter power in W,  $G$  is the antenna gain,  $A_e$  is the antenna effective aperture in  $\text{m}^2$ ,  $R$  is the range in m,  $\sigma$  is the radar cross section of the scatterer in  $\text{m}^2$ , and  $L_s$  is the system loss factor ( $0 \leq L_s \leq 1$ ). When the echo is from a target (rather than

clutter), we let  $P_r = S$  (received target signal power) and  $\sigma = \sigma_t$  (target cross-section). The signal power returned from a target is then

$$S = \frac{P_t G A_e \sigma_t L_s}{(4\pi)^2 R^4}. \quad (8)$$

## 2. Signal-to-Clutter Ratio

The power in the receiver consists of the desired wire scattered signal  $S$ , the undesired components from clutter  $C$ , and thermal noise. The command wire sensor operates in conditions where the clutter power is much greater than the noise power (i.e., a clutter limited condition). Thus, we ignore the noise in comparison with the clutter. Generally, the major source of clutter is the signal reflected from the ground; although, reflections from buildings, trees, etc., also contribute.

The basic calculation that must be done is to determine whether the wire signal power is sufficiently larger than the clutter and noise powers. In other words, we must determine if the SCR is greater than the acceptable minimum value. The minimum value depends on the probabilities of detection and false alarm. Generally, about 10 dB is required. (i.e., the signal power must be a factor of ten larger than the clutter and noise powers). Because of the independent sources of clutter and noise, the two problems can be addressed separately.

Given the standard radar range equation as a first approximation, the signal power (i.e., wire scattered power) is

$$S \approx \frac{P_t G_0^2 \lambda^2 \sigma_w^0 L L_s}{(4\pi)^3 R^4} \rho L_g \quad (9)$$

where  $G_0$  is the antenna gain in the direction of the wire,  $\sigma_w^0$  is the echo width of the wire, or two-dimensional radar cross section in  $\text{m}^2/\text{m}$ ,  $L$  is the length of the command wire illuminated by the antenna in m,  $\rho$  is the polarization mismatch loss between wire and antenna,  $L_g$  is the propagation loss factor (round trip), and  $R$  is the range of the wire

in m. The propagation loss includes reflection loss at the surface and attenuation through the ground. The equation is not very accurate because the sensor may be in the near-scattered field of the wire.

A similar approach gives the clutter power

$$C \approx \frac{P_t G_0^2 \lambda^2 \sigma^o A_c L_s}{(4\pi)^3 R^4} \quad (10)$$

where  $\sigma^o$  is the ground radar cross section per square meter in  $\text{m}^2/\text{m}^2$  and  $A_c$  is the clutter area illuminated by the antenna in  $\text{m}^2$ .

From the equations, various tradeoffs can be observed. Firstly, the SCR is independent of transmit power. Although increasing the transmit power increases the wire return, it also increases the clutter power. In addition, a narrow beamwidth antenna reduces the clutter area but can also reduce the amount of wire return, depending on how the wire is oriented.

### 3. Total Clutter Power

The total clutter power is the sum of all ground reflections arriving at the receiver. A typical scattering patch with area  $dx dz$  is shown in Figure 16.

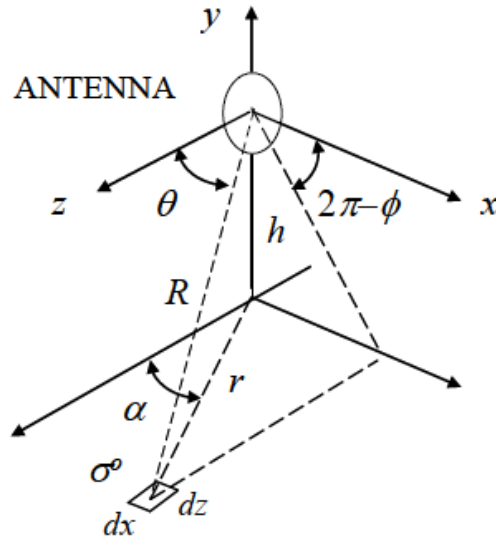


Figure 16. Backscatter from a differential ground patch (From [7])

From [7], the total clutter power from the forward half-plane ( $z > 0$ ) is defined as

$$C = \frac{P_t \lambda^2 \sigma^\circ L_x}{4\pi^2} \int_0^\infty \frac{r}{\sqrt{r^2 + h^2}^4} dr \quad (11)$$

where  $h$  is the antenna height and  $L_x$  is the cross polarization loss factor on reflection from the surface. If a minimum time gate is used, the total clutter power is further reduced to

$$C \approx \frac{P_t \lambda^2 \sigma^\circ L_x}{32\pi \sqrt{R_{\min}^2 + h^2}}. \quad (12)$$

where  $R_{\min}$  corresponds to the range at the start of the time gate, as discussed in the next section.

## C. TIME GATING

### 1. Radar Range Gating

Range gating is a process whereby the range or time is quantized into small intervals, eliminating the loss of range information and the collapsing loss [13]. A range gate is a movable gate used to select radar echoes from a very short-range interval. The range gating process consists of sampling the received signal at a specified time after the transmit pulse has been radiated. The sample period should be equal to the length of the transmitted pulse so that the maximum amount of pulse energy and the minimum of noise are incorporated into each sample.

The width of the range gate depends upon the range accuracy desired, but it is usually on the order of the pulse width. Range resolution is established by gating. Once the radar return is quantized into range intervals, the output from each gate may be applied to a narrowband filter since the pulse shape need no longer be preserved for range resolution. A collapsing loss does not take place since noise from the other range intervals is excluded.

## 2. Time Gating for Wire Detection

Time gating is basically the same as range gating. A side view of the antenna footprint on the ground is shown in Figure 17.

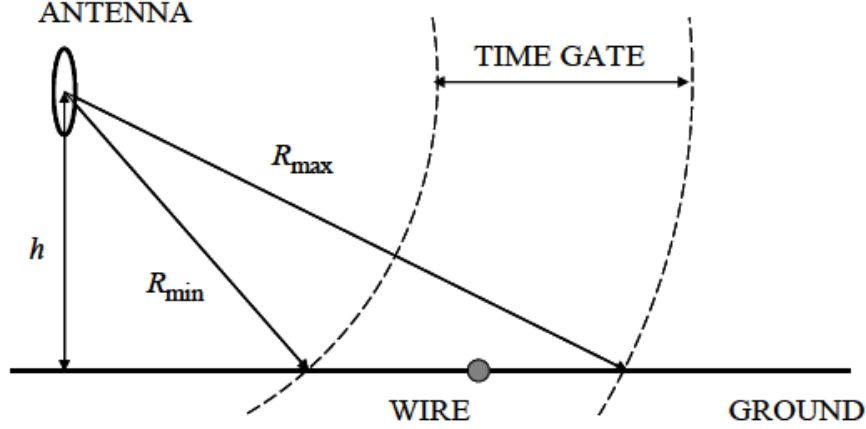


Figure 17. Time gating to reduce clutter (From [7])

Due to the short range and high grazing angle, the area close to the antenna has the most clutter return [7]. This is because surface reflection is the highest near the normal incidence. However, as that the command wire sensor is only interested in detecting wires at a distance and not the close returns, time gating is a process that can be employed. The receiver is blanked or switched off except for a prescribed period of time that corresponds to the distance or ranges of interest. The receiver is switched back on during the time that the first returns of interest from range  $R_{\min}$  arrive. As a result, the surface clutter power from ranges shorter than  $R_{\min}$  does not compete with the signal power, improving the SNR.

## D. PROBABILITIES OF DETECTION AND FALSE ALARM

### 1. Threshold Detection

A radar receiver attempting to detect a weak echo signal is limited by the presence of clutter and noise that occupies the same frequency spectrum as the target signal [14]. The minimum detectable signal  $S_{\min}$  refers to the weakest signal that can just be detected

by a receiver. The use of  $S_{\min}$  is not the preferred method to describe the ability of a radar receiver to detect echo signals from targets. Instead, the SNR or SCR is a better measure of a radar's detection performance.

In order to detect a radar signal, it is necessary to first establish a threshold at the output of the receiver. A target is considered present if the receiver output is large enough to exceed the threshold value. If there is not a large enough amplitude at the receiver output to cross the threshold, then only noise can be considered present. Threshold detection with the output of a radar receiver as a function of time is illustrated in Figure 18. The fluctuating appearance of the output is due to the random nature of receiver noise and changing clutter properties. The clutter time variation can be due to the variations in terrain scattering as the radar moves or the motion of clutter itself (e.g., trees in the wind).

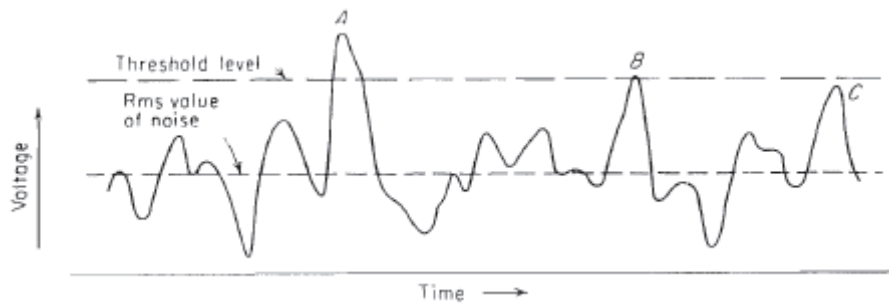


Figure 18. Envelope of radar receiver output (From [14])

The presence of a large echo signal can be identified based on its amplitude with respect to the rms noise level. The receiver output should not normally exceed the threshold level with only the presence of clutter and noise provided that the detection threshold level is set correctly. The receiver output only exceeds the threshold if a strong target echo signal is present along with the noise and clutter. However, if the threshold level is set too low, noise and clutter may exceed the threshold and be mistaken for a target, causing a false alarm. Although setting the detection threshold higher reduces the chance of noise or clutter causing false alarms, it also results in the inability to detect weak targets echoes that might not exceed the threshold. This is called a missed detection.

## **2. False Alarms**

A false alarm is an erroneous radar target detection decision caused by noise, clutter, or other interfering signals exceeding the detection threshold. In general, it is an indication of the presence of a radar target when there is no valid target. A typical radar operates in noise limited environment, and a statistical model of thermal noise is appropriate. On the other hand, the command wire sensor will be operating in a clutter limited condition. The clutter return will be constant in time only if the radar is stationary and viewing in a constant environment such as the desert. If the sensor is moving over a uniform terrain, the clutter will be time invariant.

Consider a detection scenario whereby only one target (a command wire) is present in a uniform terrain. There will be a high probability of detection and a zero false alarm rate. However, if the command wire is placed along with other telephone or electrical wires, the probabilities of detection and false alarm rate will deteriorate greatly. Hence, in order to mitigate this, some type of constant false alarm rate (CFAR) receiver is required. CFAR automatically raises the threshold level to keep clutter echoes and external noise from overloading the processor with extraneous information. The threshold level is adjusted to keep the false alarm rate constant.

## **E. SIMULATION RESULT**

Based on the models developed, the simulation results were presented in [7]. Grid contours were generated by taking multiple line paths. A typical result for two frequencies for a 100 meter wire is shown in terms of power contours over a grid of observation points in Figures 19 and 20. Due to symmetry, only data from a grid over half of the wire needs to be computed. This is illustrated by the blue shaded box in the insert of Figure 20. In addition, data for a rotated wire can be obtained by a rotation and translation of the data computed for  $\alpha = 0^\circ$ . The data are representative of a wide range of sensor scenarios. The signal level at 150 to 200 meters from the wire is typically in the  $-125$  dBW to  $-135$  dBW range for a transmit power of 0.011 W. The signal level increases directly with transmit power, but so does the clutter.

The peak scattering from a straight wire normally increases with frequency. Simulations show that the highest signal power appears to occur at the lower frequency of 300 MHz. This is a consequence of operating in the near field of the wire where the incident wave is spherical. In order to fulfill the standard far-field criterion of  $2L^2 / \lambda$ , the sensor has to be 20 km distant at 300 MHz and more than 67 km at 1 GHz.

An estimate of the clutter levels based on several values of  $\sigma^o$  is given in Table 3 of [7]. The reported values of  $\sigma^o$  vary widely in the literature, as noted in [7]. For favorable (i.e., low) values of  $\sigma^o$ , the resulting SCRs for the contours shown in Figures 19 and 20 are in the range of 0 to 10 dB.

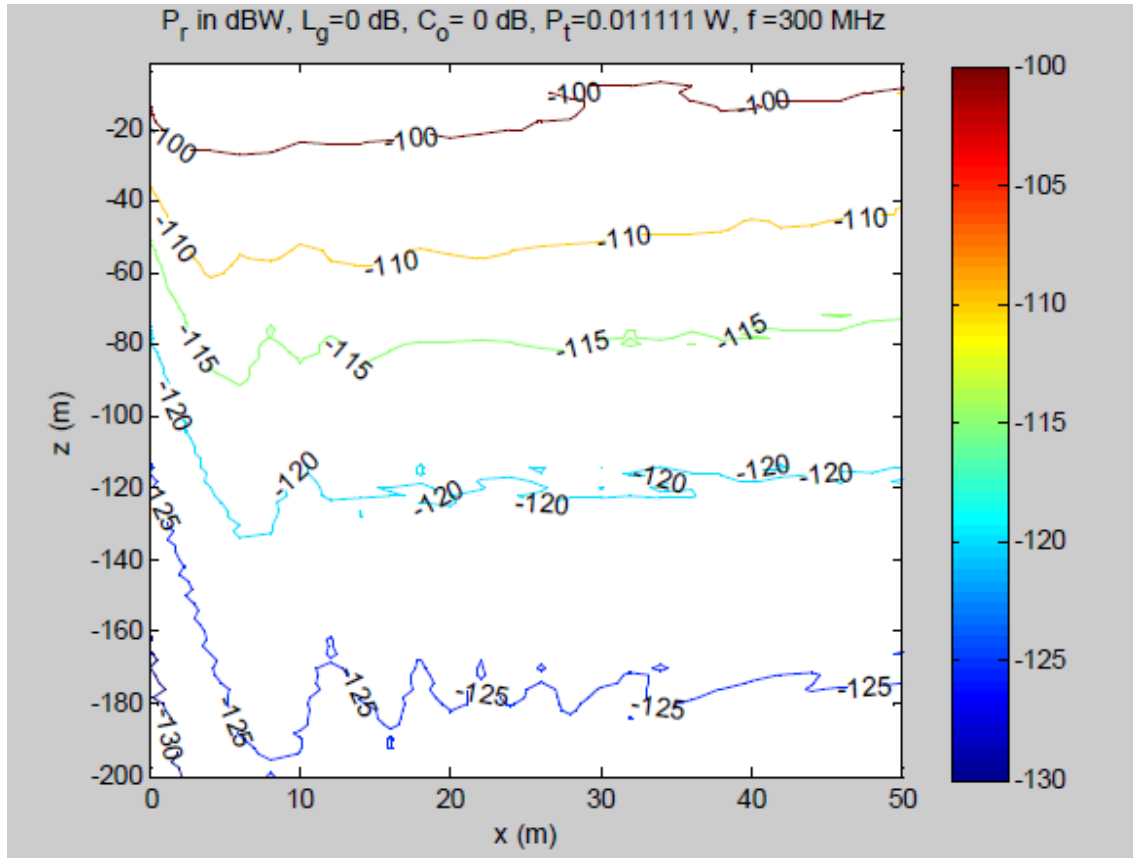


Figure 19. Typical power contours for wire scattering at 300 MHz (From [7])



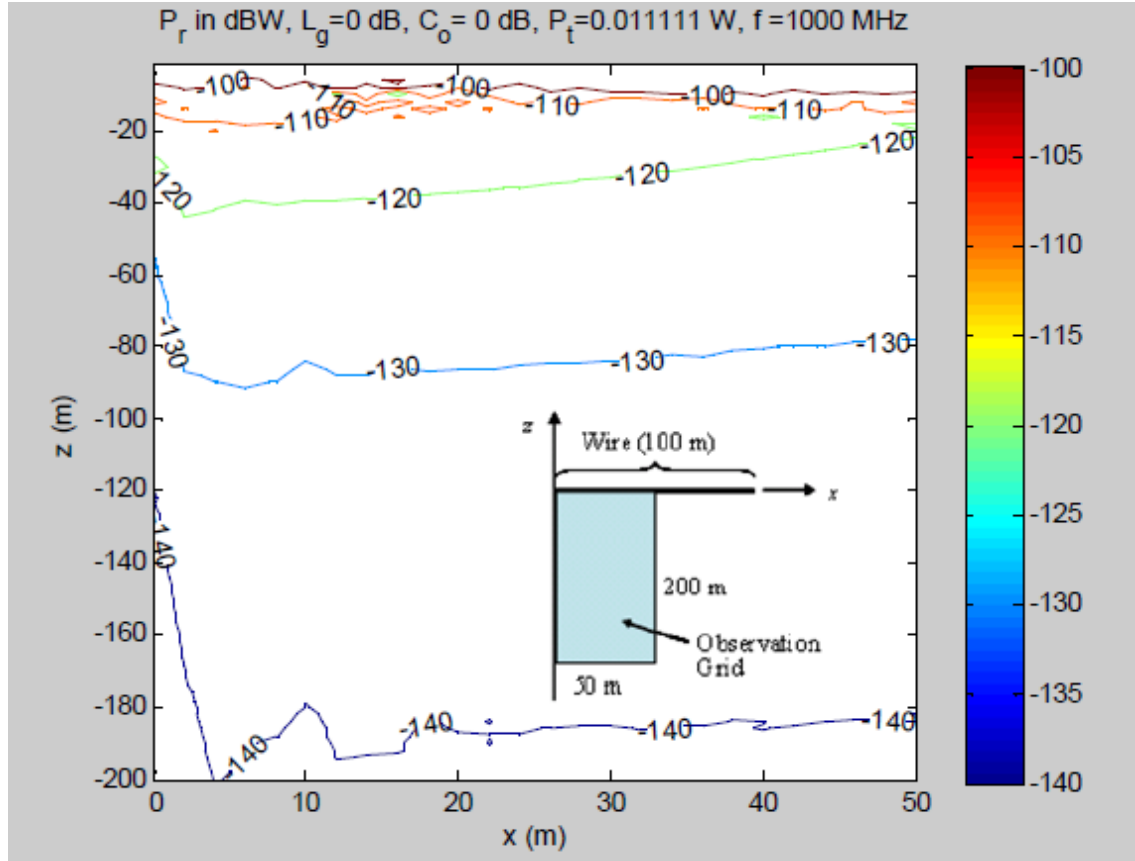


Figure 20. Typical power contours for wire scattering at 1 GHz (From [7])

## F. SUMMARY

In order to detect the command wire, it is important to understand the various wire scattering theories and clutter modeling. The SCR equations highlighted key tradeoffs with respect to transmit power, wire return and clutter power, as well as beamwidth. Simulations and measurements are necessary to further examine the wire scattering characteristics for a command wire sensor. The measurement results are presented in the next chapter.

THIS PAGE INTENTIONALLY LEFT BLANK

## IV. MEASUREMENT RESULTS

In this chapter, the measurement setup, including chamber dimensions and hardware specifications, are presented. The antenna pattern measurement results are presented, followed by an investigation of the transmit–receive interference issue. The effectiveness of time gating in measuring the RCS of a target is also considered. Lastly, comparison plots between different types of targets, as well as different wire orientation, with and without background subtraction, are presented.

### A. TEST SETUP

#### 1. Chamber Dimensions

The NPS anechoic chamber is located in Spanagel Hall, Room 604. Although the chamber was built for instruction purposes only, it can be used for research as well. The chamber is shown in Figure 21, and all dimensions are in inches.

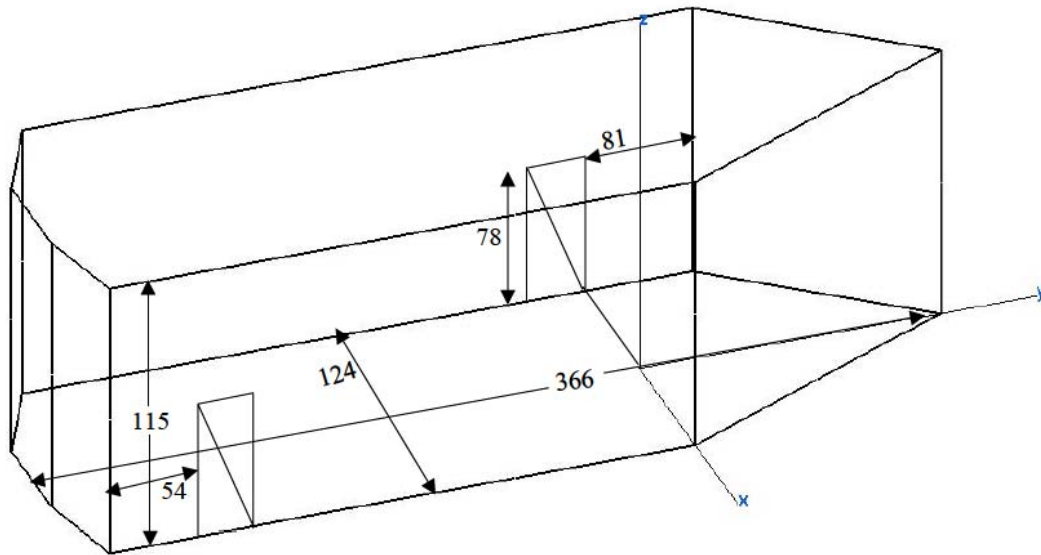


Figure 21. Specifications of the anechoic chamber at the Naval Postgraduate School (From [21])

From [21], the quality of the radiation patterns from the chamber is not as good as desired for research studies, and this is mainly due to multiple reflections from the walls. The walls in the wedge-shaped part of the chamber act like a corner reflector and create a hot spot in the chamber which can corrupt pattern measurement. There is only a thin foil layer between the absorber and the wall, and there are regions where there is no foil at all. Hence, the chamber is not a well-designed for performing sensitive pattern measurements and making low noise or interference measurements.

## 2. Antenna Dimensions

The antenna used for the measurements is the Sylvania pyramidal ridged horn antenna, with a bandwidth of 4 to 18 GHz. The ridged horn has fins attached to the inside of the horn, extending down the center of the sides. The fins inside the mouth of the horn lower the cutoff frequency, increasing the antenna's bandwidth. In addition, the horn antenna provides a significant level of directivity and gain. The dimensions of both the transmit and receive horn antennas used for the command wire sensor measurements inside the anechoic chamber are shown in Figure 22. All the dimensions are in centimeters.

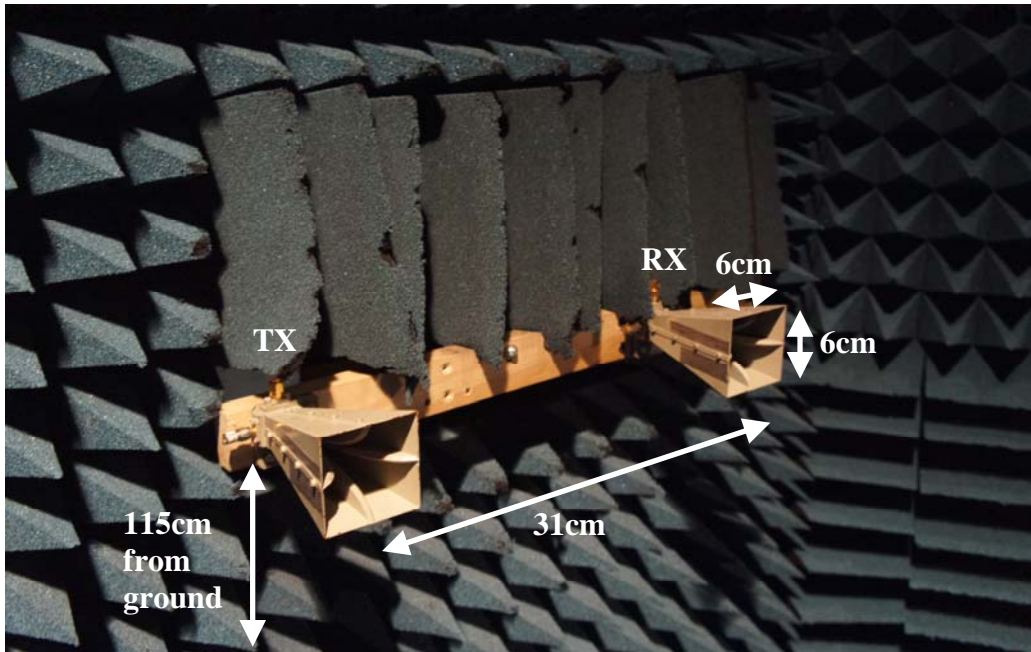


Figure 22. Transmit and receive horn dimensions

The horns shown in Figure 22 are vertically polarized. Due to equipment limitations, the antennas are fixed to only face horizontal and cannot be tilted upwards or downwards. The transmit and receive horns also cannot be placed further away from each other (more than 31cm) due to mounting limitations.

### 3. Equipment Setup

The test equipment setup is shown in Figure 23. The distance between the transmit horn and the pedestal at the end of the chamber is approximately 19 feet (5.8 meters), and there is an estimated 69 dB path loss between the horn and pedestal. The transmit horn inside the chamber is connected to a directional coupler (HP87300C), an amplifier (HP8348A), a vector network analyzer (HP8510), and a frequency convertor (HP8511). There is a 25 dB pad installed between the directional coupler and the reference port of the frequency convertor. The cable loss for this path is approximately 8.8 dB.

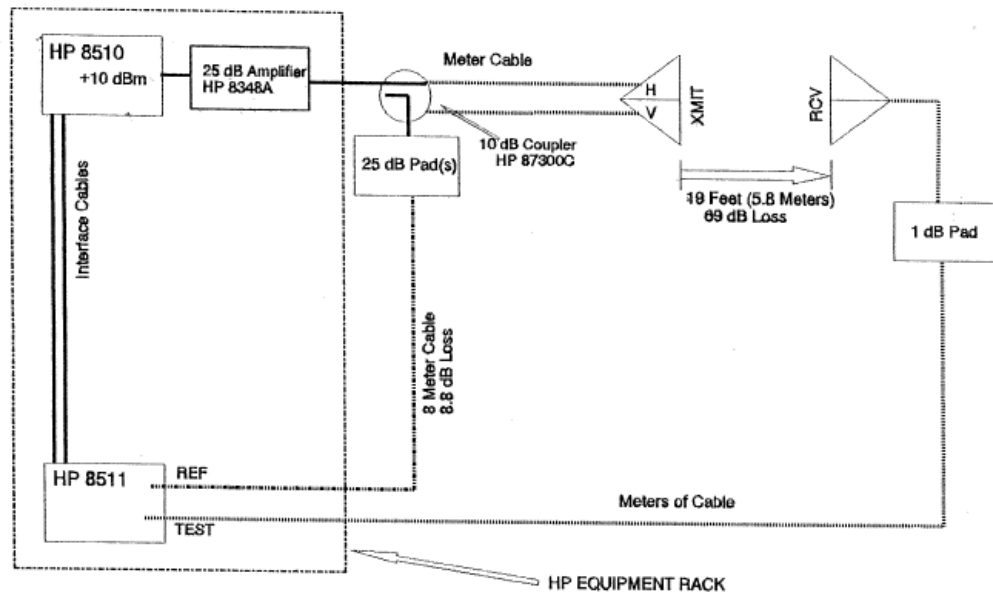


Figure 23. Test equipment setup

## B. BEAMWIDTH MEASUREMENTS

### 1. Equipment Setup

The antenna model used is the Sylvania AN-48. As the specifications of the antenna cannot be found online, due to obsolescence, it was necessary to perform the antenna beamwidth and gain measurements. The equipment setup is shown in Figure 24. The transmit horn was placed on the wall, whereas the receive horn was placed on the pedestal, located approximately 19 feet away from the transmit horn. The pedestal was programmed to rotate from -90 degrees to the left to +90 degrees to the right. In this way, the receive antenna was able to capture the transmit antenna beam profile, and hence, determine the beamwidth.

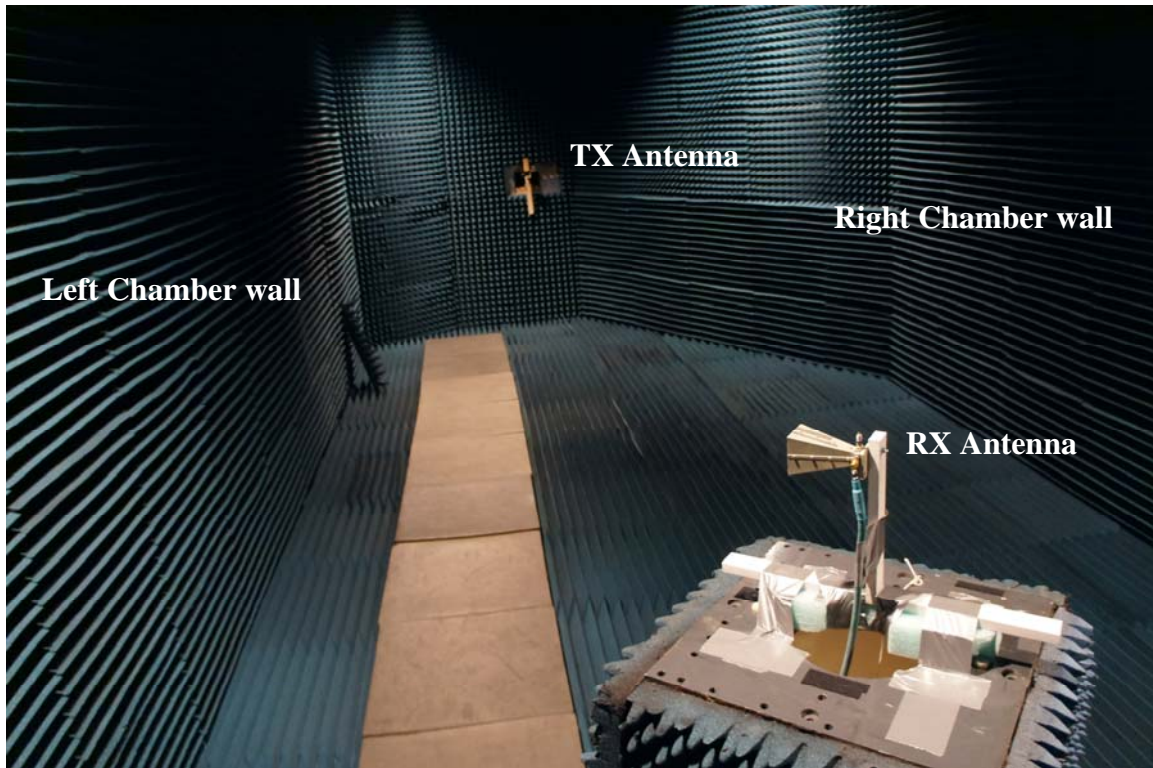


Figure 24. Antenna beamwidth measurement

## 2. Beamwidth Plots

The measured antenna patterns at 4, 5, and 6 GHz are shown in Figures 25, 26 and 27, respectively. The 3 dB beamwidth is approximately equal to the angle from the peak of the power to the first null. From Figures 25 and 26, it can be seen that the radiation pattern is not symmetrical. This is due to the wall shape of the anechoic chamber, as can be seen in Figure 24. The shape of the left chamber wall is not proportionally symmetrical to the right chamber wall. Therefore, in order to determine an accurate antenna beamwidth, only the left half of the pattern is taken into consideration. Hence, the determined antenna beamwidth for the Sylvania AN-48 pyramidal ridged horn antenna are  $72^\circ$ ,  $60^\circ$  and  $48^\circ$  at 4 GHz, 5 GHz and 6 GHz, respectively.

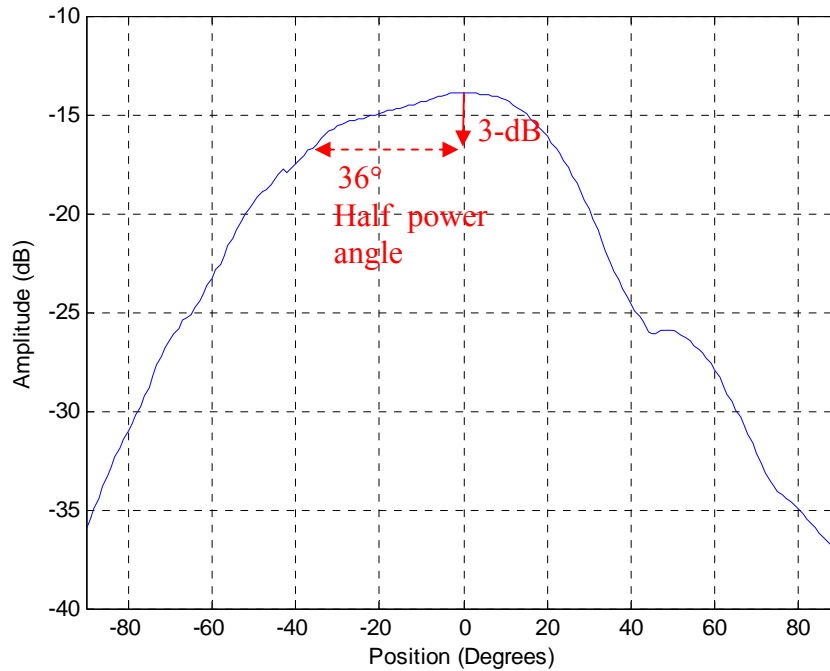


Figure 25. Antenna beamwidth at 4 GHz

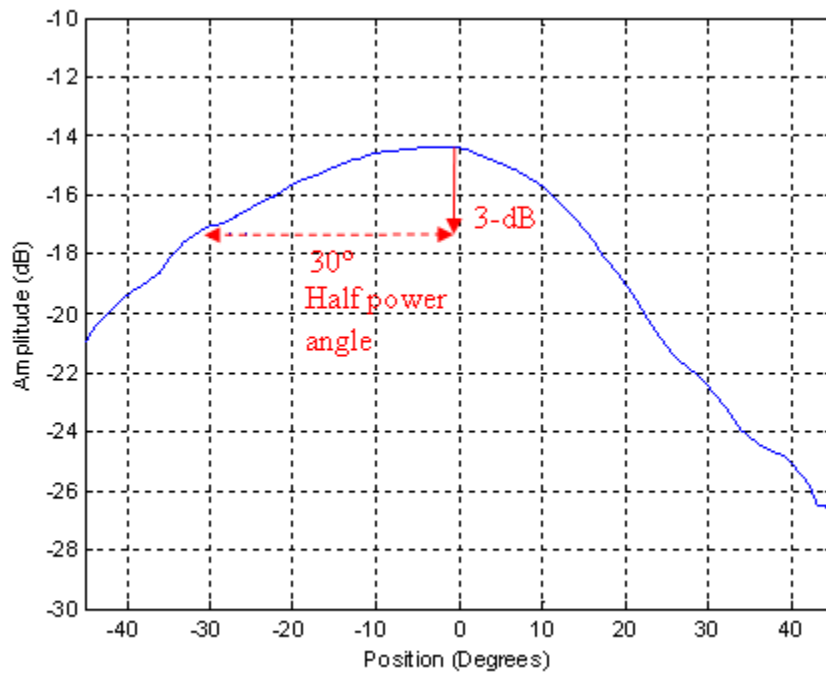


Figure 26. Antenna beamwidth at 5 GHz

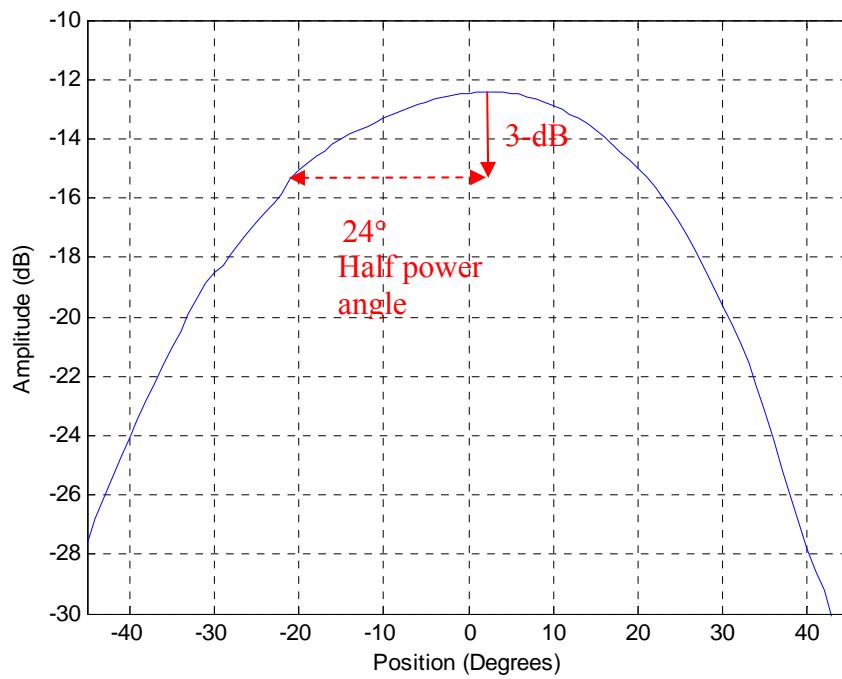


Figure 27. Antenna beamwidth at 6 GHz



## C. HORN LEAKAGE

### 1. Chamber Ambient

The anechoic chamber ambient measurement from 4 to 6 GHz is shown in Figure 28. From the plot, it can be observed that the ambient (background return) is around  $-17$  dB from 4 to 5 GHz and starts to dip to  $-33$  dB at 5.5 GHz.

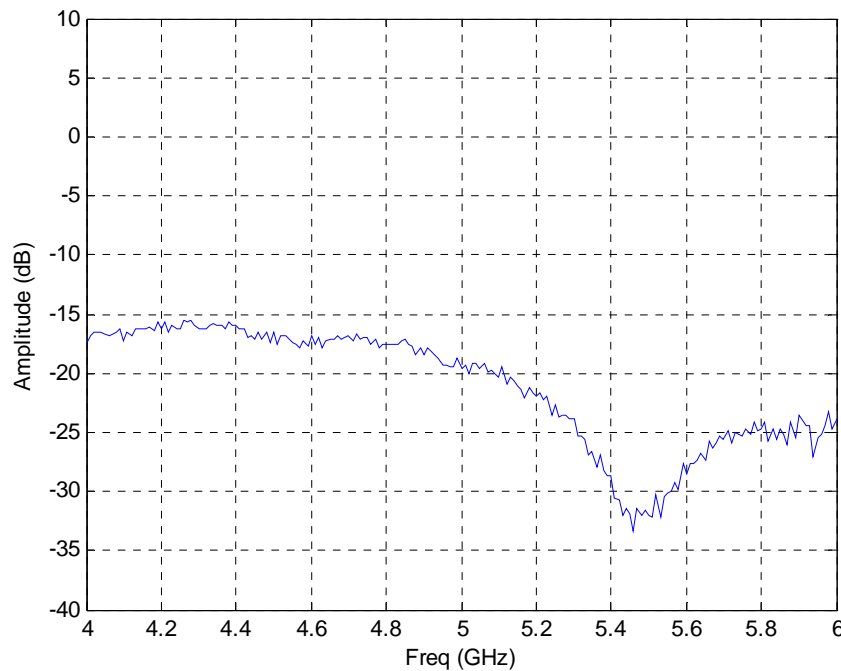


Figure 28. Anechoic chamber Ambient 4 – 6 GHz

The ambient reading is unusually high for an empty chamber reading. It was suspected that there might be some leakage contributing to the reading. The ambient for an empty chamber should approximately be  $-30$  dB. Due to the close distance between the transmit and receive horn (31 cm), transmit-receive leakage is suspected. The close proximity between the two horns causes some of the power to leak directly from the transmit horn to the receive horn. The two horns cannot be placed further apart due to chamber limitations. Hence, an absorber must be placed in between the two horns to reduce the leakage experienced by the receive horn.

## 2. Leakage Reduction

In order to reduce the leakage from the transmit antenna, a radar absorbing material (RAM) was placed in between the transmit and receive horn. ECCOSORB RAM foam is a series of lightweight, free space, multi-layer, broadband microwave absorbers. It is made from polyurethane foam that is treated with carbon and assembled in a laminate construction to generate a controlled conductivity gradient. It can be used to produce desired modifications in antenna patterns such as the reduction of side-lobes and back-lobes. Examples for use are radar antenna nacelles, anechoic enclosures, antenna or target test mounts in radar ranges, and inside or outside horn antennas.

Due to the close distance (31cm) between the two horns, the number of RAM layers that can be placed in between is limited. Measurements were done to compare the ambient reduction with one to three layers of RAM added. The front view with one piece of RAM inserted between the transmit and receive horn is shown in Figure 29. The side view of two pieces of RAM between the two horns is shown in Figure 30.

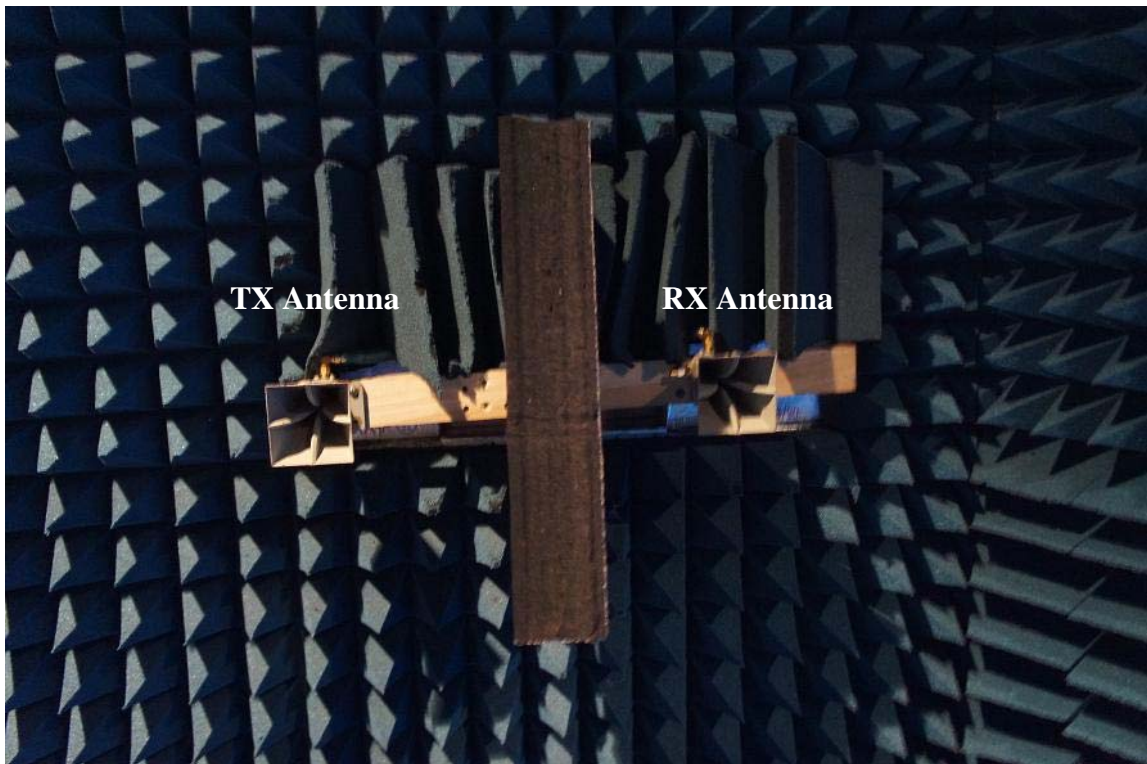


Figure 29. One piece of RAM inserted between Tx and Rx horns (front view)

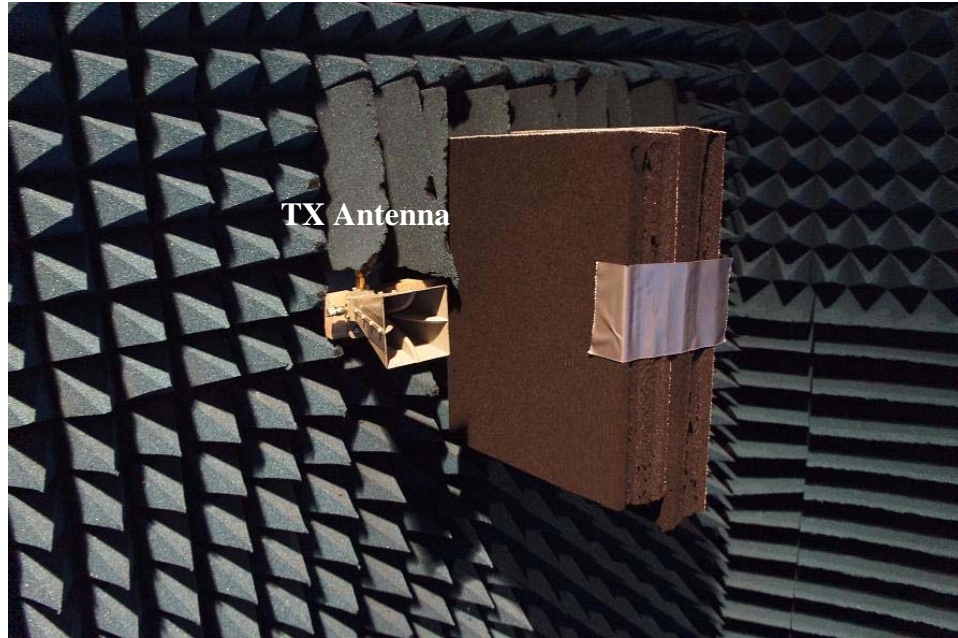


Figure 30. Two pieces of RAM inserted between Tx and Rx horns (side view)

The plots in Figures 31 to 34 show the chamber ambient measurements with different layers of RAM inserted between the horns. It can be seen clearly that the RAM insertion reduced the leakage. There is approximately a 12 dB reduction with one and two pieces of RAM inserted, as shown in Figures 31 and 32. Adding in three pieces of RAM reduces the leakage by 15 dB. However, it is very difficult to secure three pieces of RAM in the tight 31 cm gap. In addition, three pieces of RAM bundled together is too heavy and cannot stay firmly in place. From Figure 34, it can be seen that the difference between inserting two or three pieces of RAM is not very great; hence, for the command wire measurements, two pieces of RAM were used to reduce the leakage between the transmit and receive horns.

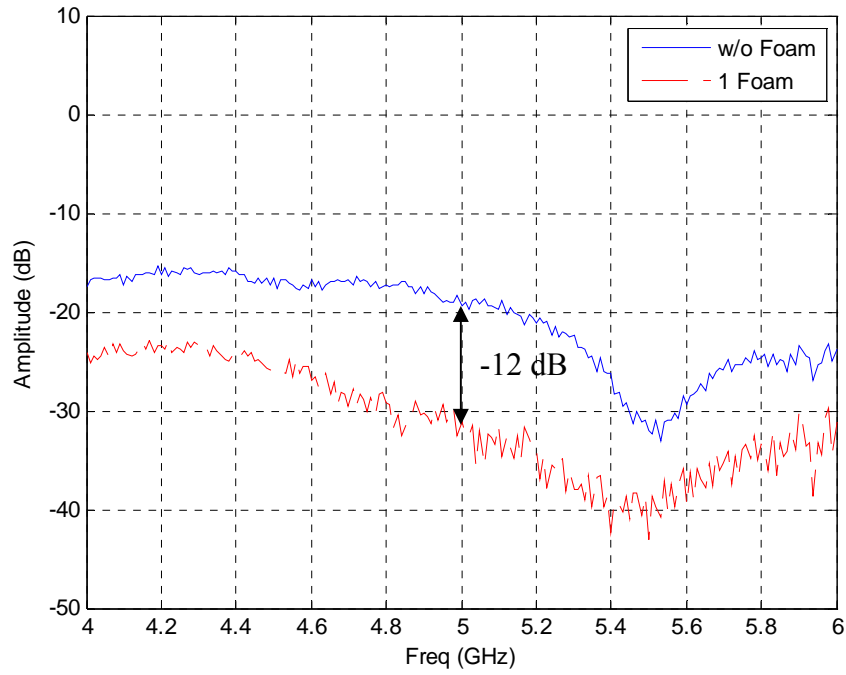


Figure 31. Chamber ambient with one piece of RAM and without RAM

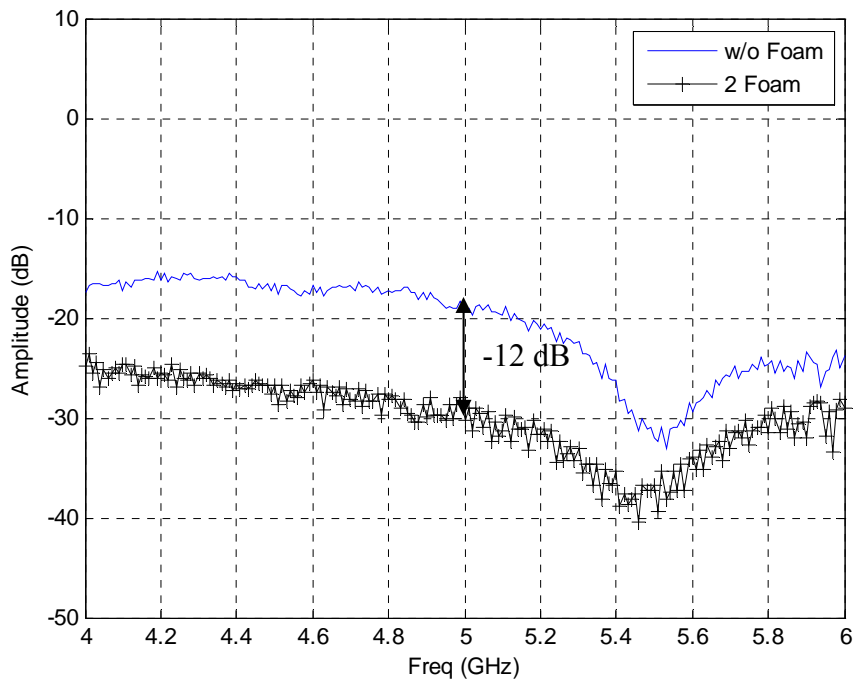


Figure 32. Chamber ambient with two pieces of RAM foam and without RAM

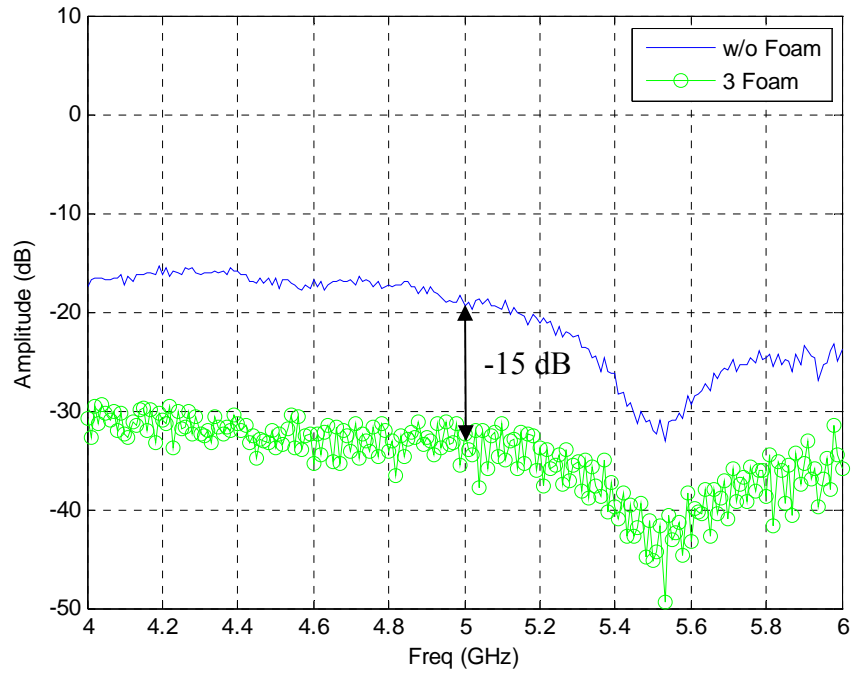


Figure 33. Chamber ambient with three pieces of RAM and without RAM

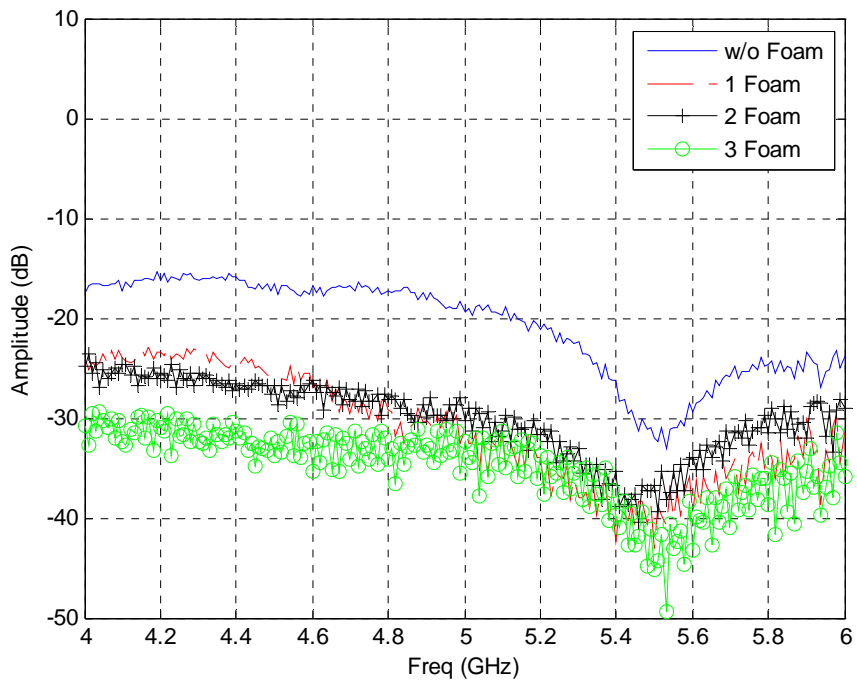


Figure 34. Chamber ambient comparison for zero to three pieces of RAM



## D. WIRE SCATTERING MEASUREMENTS

### 1. Initial Wire Measurements

A three-meter American wire gauge (AWG) 8 wire was horizontally laid across the width of the chamber, five meters away from the antenna, as illustrated in Figure 35. The reason for laying the wire five meters instead of six or seven meters is due to the pedestal. The pedestal is located six meters away from the antenna, and placing the wire on the pedestal or further away affects the wire's scattering returns. The wire was laid to simulate a command wire on the ground, and the purpose of this measurement was to try to pick up the scattering of a thin wire from the ground.

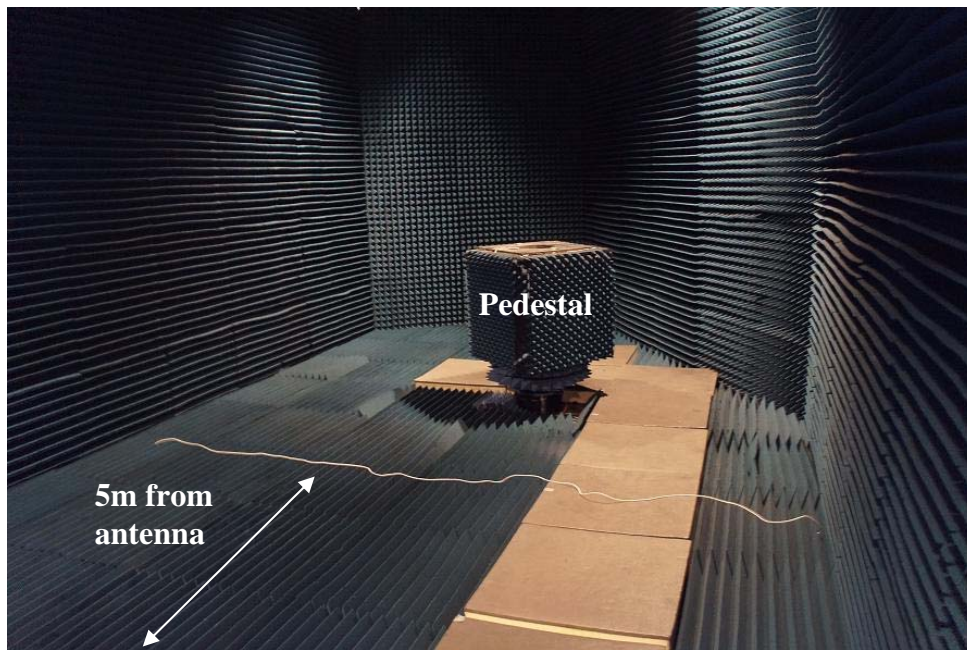


Figure 35. Wire laid horizontally across the width of the chamber, five meters from the antenna

A wire scattering measurement was done from 4 GHz to 6 GHz, and a coherent subtraction of the stored background signal performed. The results are shown in Figure 36. As can be seen from the plot, the residual scattering from the wire is very small, less than 1 dB. The measured result is consistently low, with no significant peaks observed. Note that the antenna is vertically polarized, so the wire scattering is expected to be very

small. An initial concern was that the antenna beamwidth might not be able to pick up the wire on the ground, as the antenna is unable to be tilted downwards.

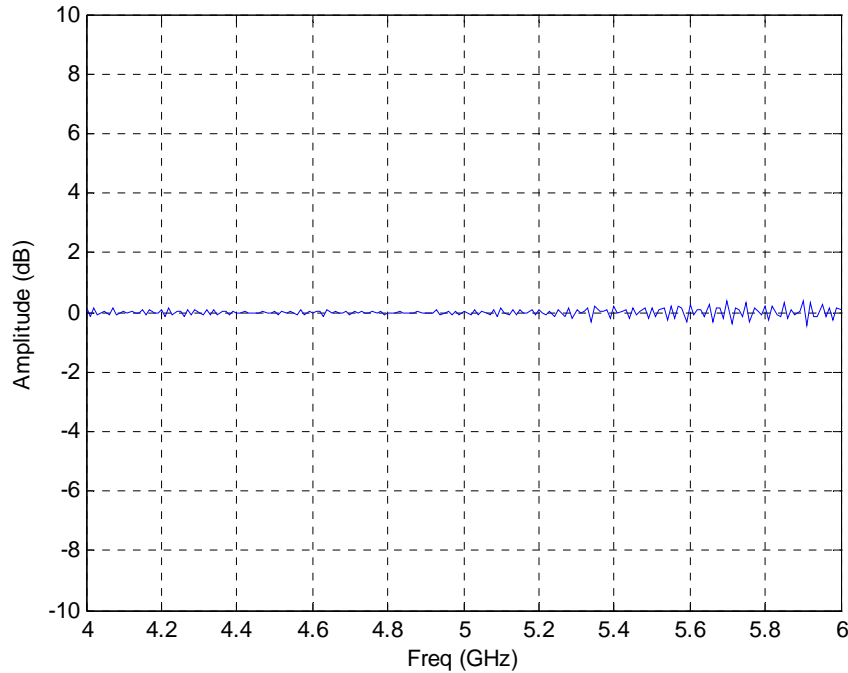


Figure 36. RCS of a wire laid horizontally across the chamber, five meters from the antennas

As the antennas cannot be tilted downwards, the wire aspect angle was changed by hanging the wire vertically down from the ceiling, as shown in Figure 37. By hanging the wire vertically down from the ceiling, the wire is positioned to be directly in line-of-sight (LOS) to both the transmit and receive antennas. The wire was now aligned with the horn polarization. The position of the wire was six meters away from the antenna, which is just above the pedestal. The residual scattering from the wire is shown in Figure 38. There is a slight improvement, as compared to the case of the wire laid on the ground in Figure 36. From Figure 38, the difference is approximately 1 dB, but this reading is not significant enough to be useful for a command wire sensor in a clutter environment.



Figure 37. Wire hung vertically from the ceiling, six meters from the antenna

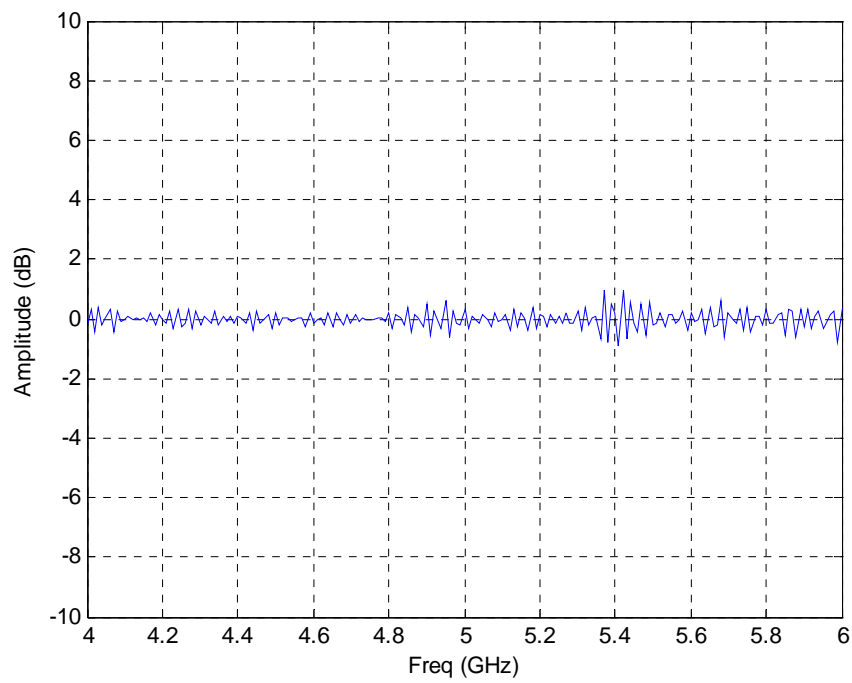


Figure 38. Residual scattering from a wire hung vertically from the ceiling, six meters from the antenna



## 2. Plate Measurements

In order to estimate the wire RCS, a calibration target is needed. The RCS of a square metal plate is used for this purpose. The monostatic RCS is approximately a “sinc” function with a half power beamwidth [22]

$$HPBW = \frac{\lambda}{2d} . \quad (13)$$

where  $d$  is the edge length, and the result is in radians.

Using Eq. (13) at 5 GHz (wavelength of 0.06 meters), we used a Matlab program to determine the dimensions of a plate to give a beamwidth of  $8^\circ$  so that both horns are in the HPBW of the scattering from the plate. The edge length  $d$  of the square metal plate was calculated to be 0.22 meters. A 0.22 by 0.22 metallic plate was fabricated for this measurement, as shown in the chamber in Figure 39. The RCS of a square metallic target is given by [22]

$$\sigma = \frac{4\pi A^2}{\lambda^2} . \quad (14)$$

Using Eq. (14), we calculated the RCS  $\sigma$  of the plate to be  $7.32 \text{ m}^2$ , which is equivalent to 8.646 dBsm. The fabricated plate was mounted on a wooden stand and placed onto the pedestal, six meters away from the antenna, as shown in Figure 39.

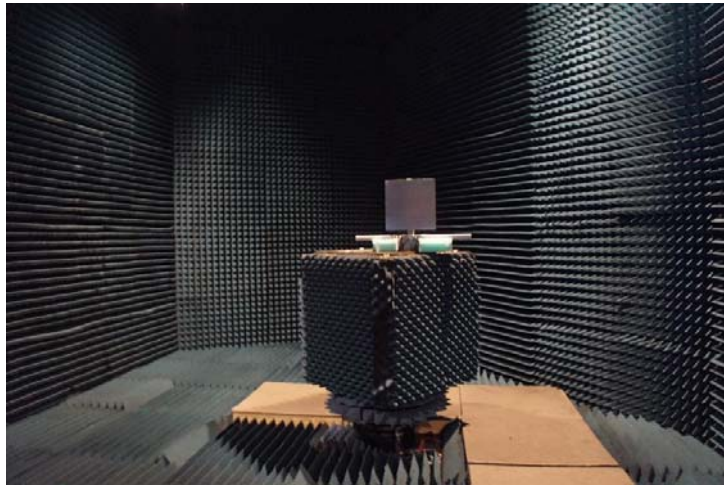


Figure 39. Square metal plate placed on pedestal, six meters away from the antenna

The measured residual for the 0.22 by 0.22 metal plate is shown in Figure 40. The result is not conclusive as it does not show consistent scattering from the metal plate. The results show rapidly fluctuating peaks from the interference between the residual signal and multipath components. The reflections can be coming from the side walls, the floor as well as the ceiling. The multipath contributes to the interference received by the receive antenna.

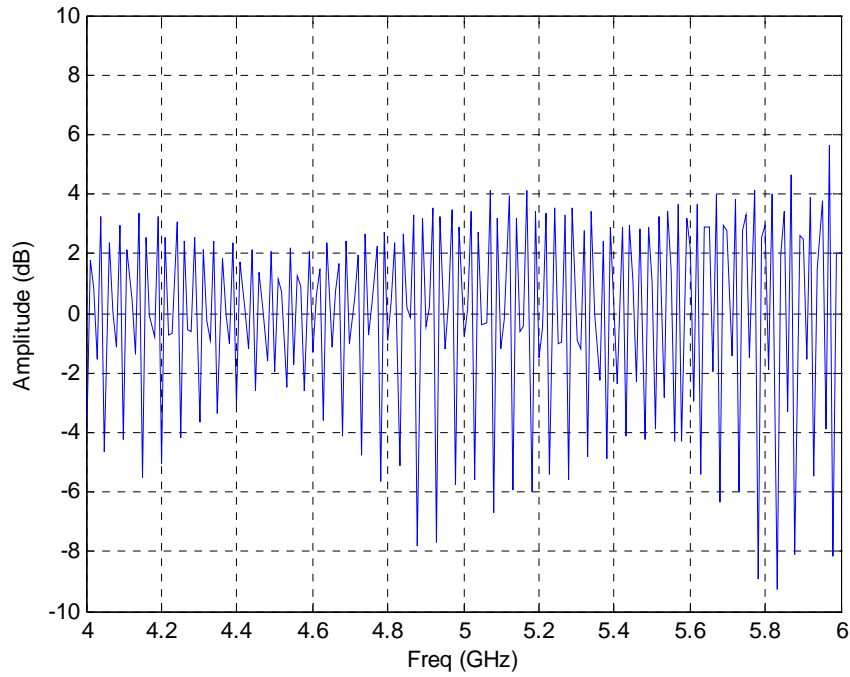


Figure 40. Measured return of 0.22 by 0.22 metal plate, placed six meters away from the antenna

### 3. Pole Measurements

As the antenna was not able to pick up the 0.22 by 0.22 meter plate, it was proposed to do a sensitivity measurement using a solid metal pole inside the chamber. The metal pole was 2.45 meters in length and 0.02 meters in diameter. The pole was placed six meters away from the antenna, as illustrated in Figure 41.



Figure 41. 2.45 meter metal pole placed vertically, six meters away from the antenna

The measurement for the 2.45 meter pole is shown in Figure 42. As expected, the results show similar multipath characteristics to the plate measurements in Figure 40. Fluctuating peaks in the range of  $\pm 1$  dB can be observed from the plot. The conclusion is that the residual multipath presence within the anechoic chamber is strong, and these reflections from the various internal walls pose a problem for measurements, as illustrated in Figure 43. Therefore, time gating was required to eliminate the multipath components.

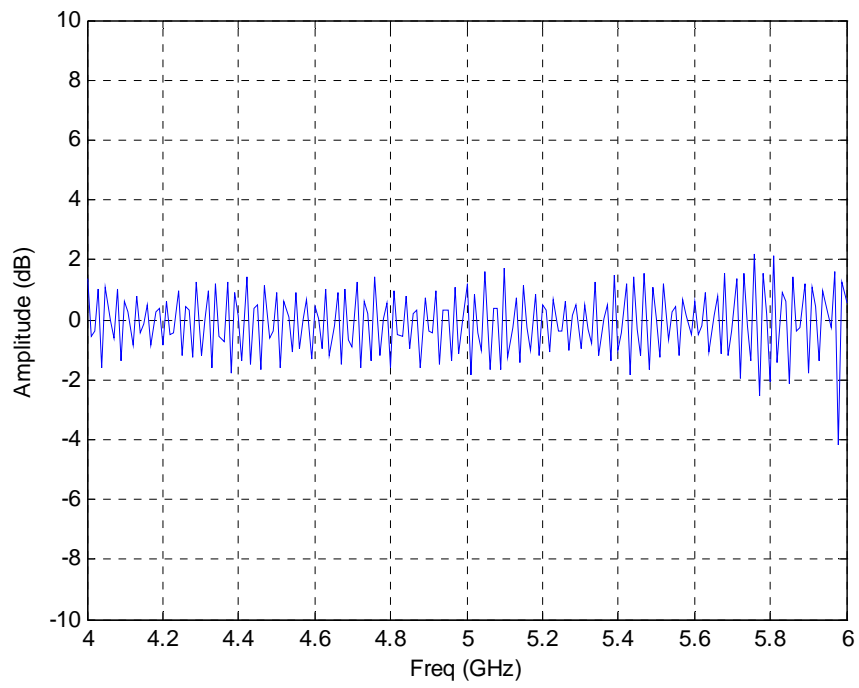


Figure 42. Return from a 2.45 meter vertical pole, placed six meters away from the antenna

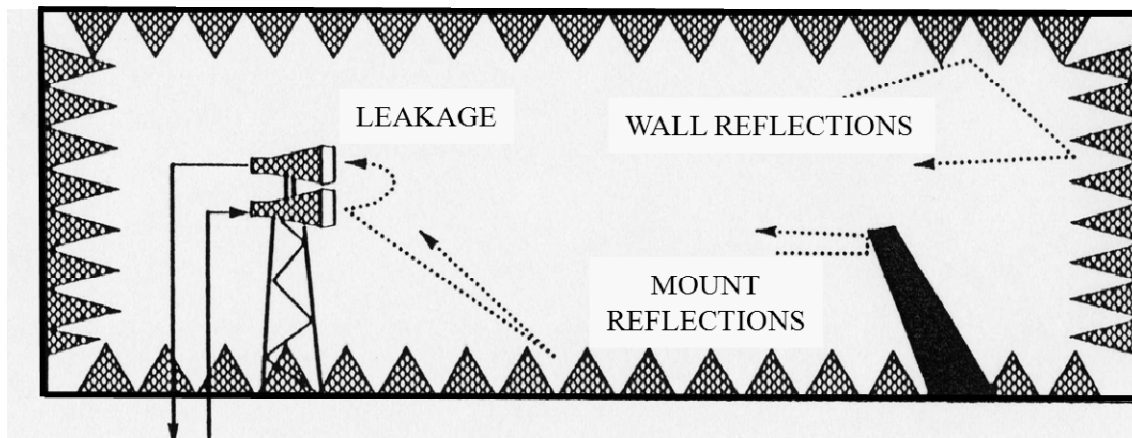


Figure 43. Multipath components within anechoic chamber

## **E. TIME GATING**

As mentioned in Chapter III, time gating is a process whereby the range or time is quantized into small intervals. The receiver is switched off except for a prescribed period of time that corresponds to the ranges of interest. As the surface clutter power from ranges outside of the prescribed period does not compete with the signal power, the end result is an improved SCR.

### **1. Time Gating Range**

In order to implement time gating for the command wire measurements, it is necessary to first determine the period of time that corresponds to the distance within the anechoic chamber. The distance between the antenna and the pedestal is approximately six meters. A metallic plate was placed exactly six meters away from the antenna, and the time gate range was set to start at 25 ns and stop at 40 ns. As shown in Figure 44, when the plate was placed in the chamber, there is an obvious peak occurring at 32.425 ns. This time corresponds to the location of the plate in the chamber, which is six meters away from the antenna. Similar measurements were done for various distances from the antenna. The plots for the various distances are shown in Figures 44 to 49. Note that when the distance between the antenna and target is too small (one meter away), it is very difficult to identify the time that corresponds to the distance, as can be seen in Figure 49.

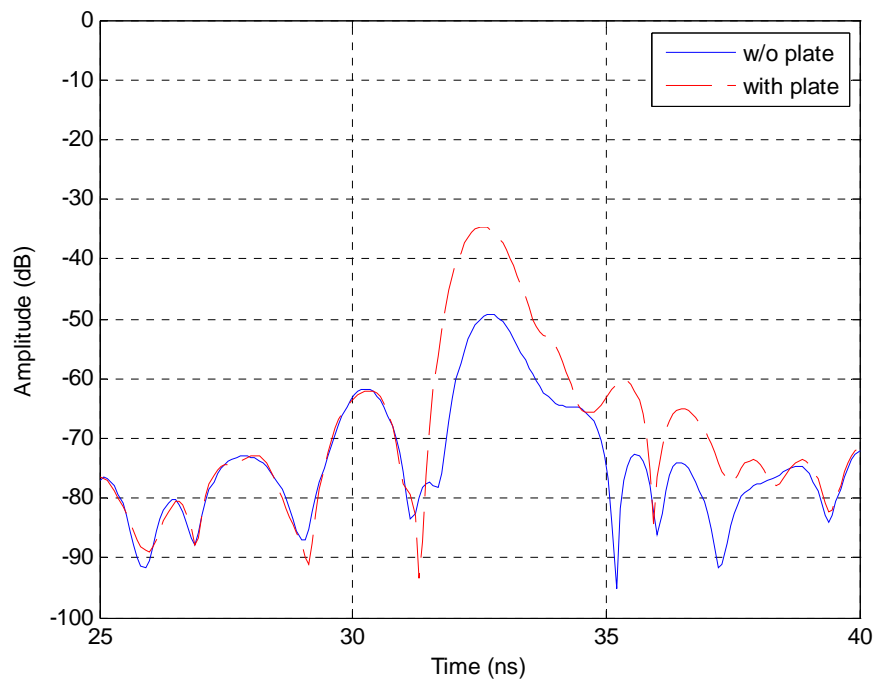


Figure 44. Time gated return for the plate six meters from the antenna, at 25 to 40 ns

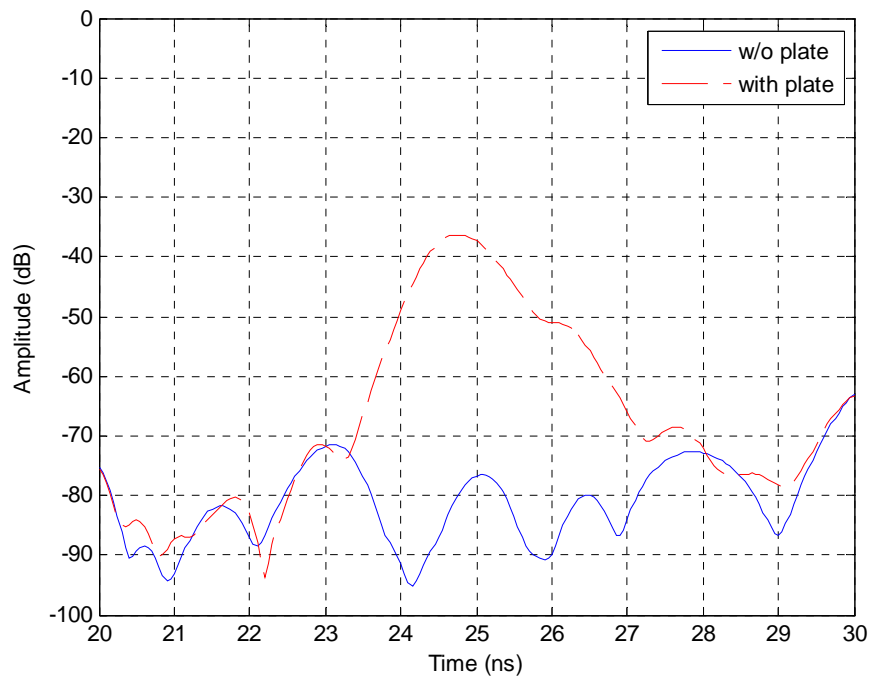


Figure 45. Time gated return for the plate five meters from the antenna, at 20 to 30 ns

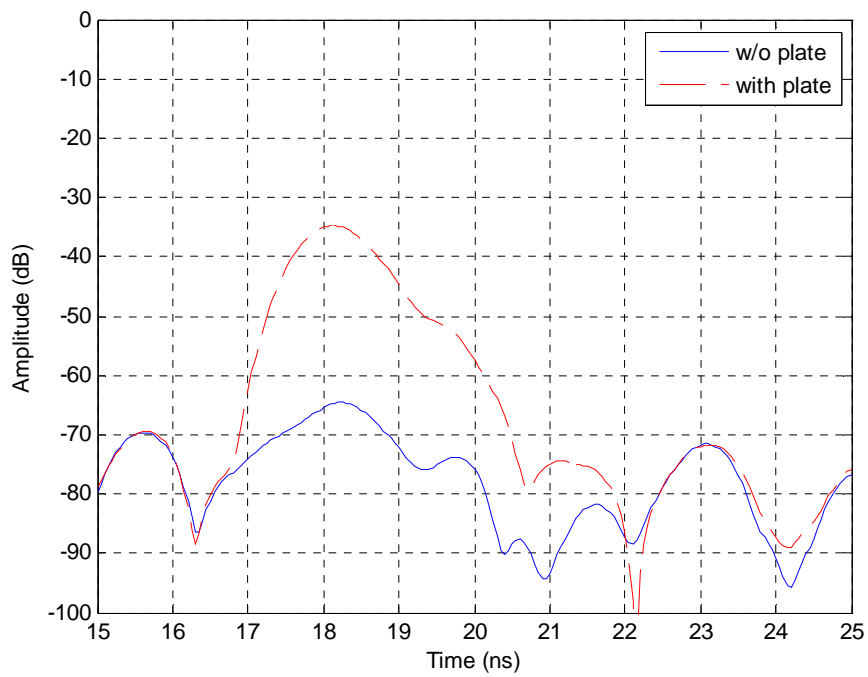


Figure 46. Time gated return for the plate four meters from the antenna, at 15 to 25 ns

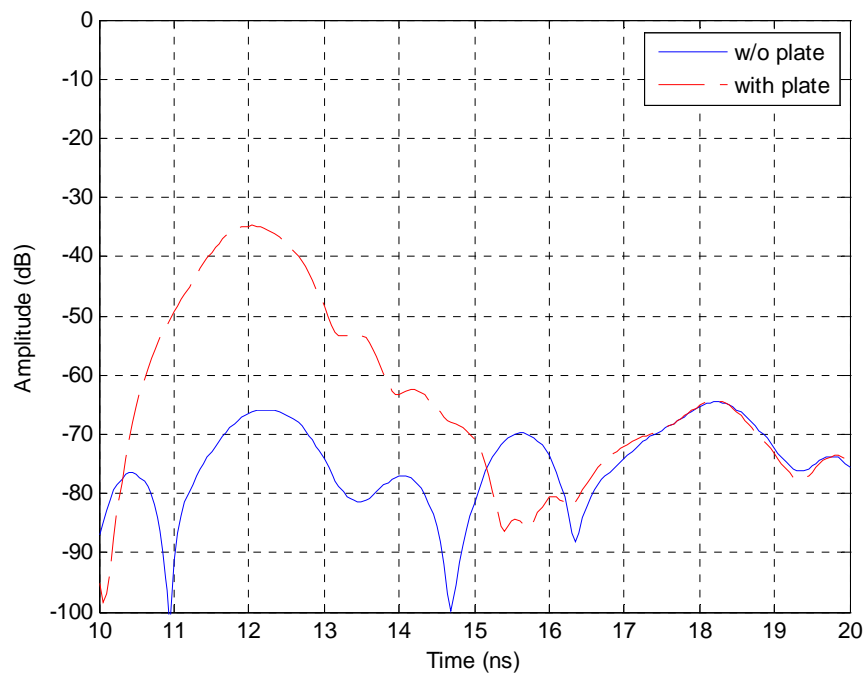


Figure 47. Time gated return for the plate three meters from the antenna, at 10 to 20 ns

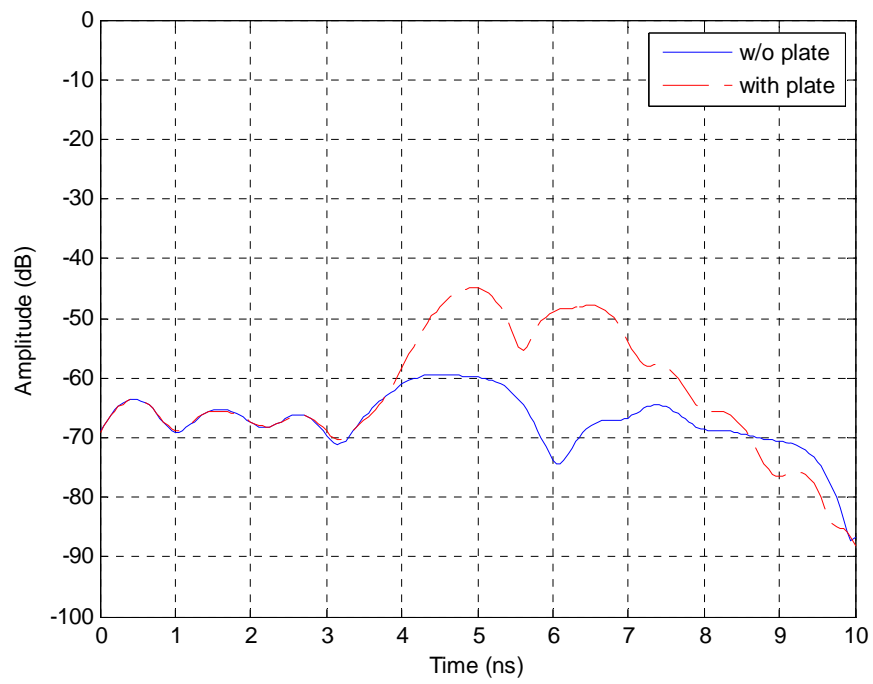


Figure 48. Time gated return for the plate two meters from the antenna, at 0 to 10 ns

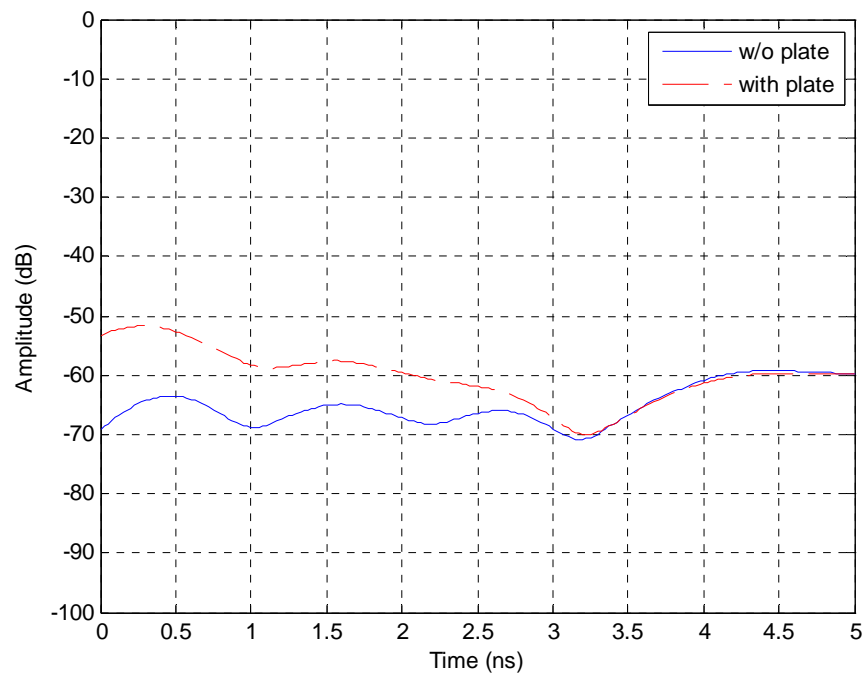


Figure 49. Time gated return for the plate one meter from the antenna, at 0 to 5 ns



After analyzing the time gate plots, the time that corresponds to the respective distances from the antenna is shown in Table 4. In addition, the gate time and corresponding distances within the anechoic chamber is illustrated in Figure 50. With this information, time gating can then be implemented for the command wire measurements, in order to achieve an improved SCR.

Table 4. Summary of time gate with distance

Distance (m)	Time (ns)	Time Gate Range (ns)
6	32.425	25 – 40
5	24.75	20 – 30
4	18.1	15 – 25
3	12.05	10 – 20
2	4.95	0 – 10
1	0.35	0 – 5

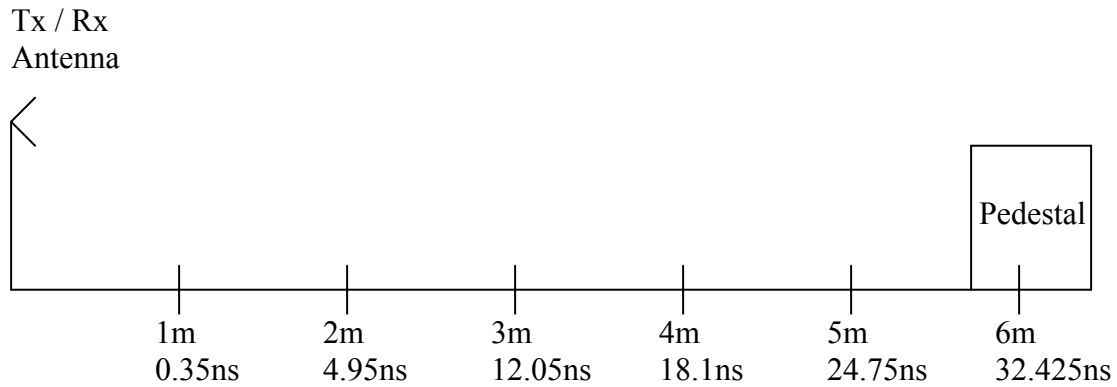


Figure 50. Time gate with corresponding distance from antenna

## 2. Measurements with Time Gating

The time gate was turned on from 25 to 40 ns, which is the gate centered at a range of six meters from the antenna. The chamber response is shown in Figure 51. Comparing this plot with the plot in Figure 32, we can clearly see that there is approximately a 20 dB drop when time gate is switched on.

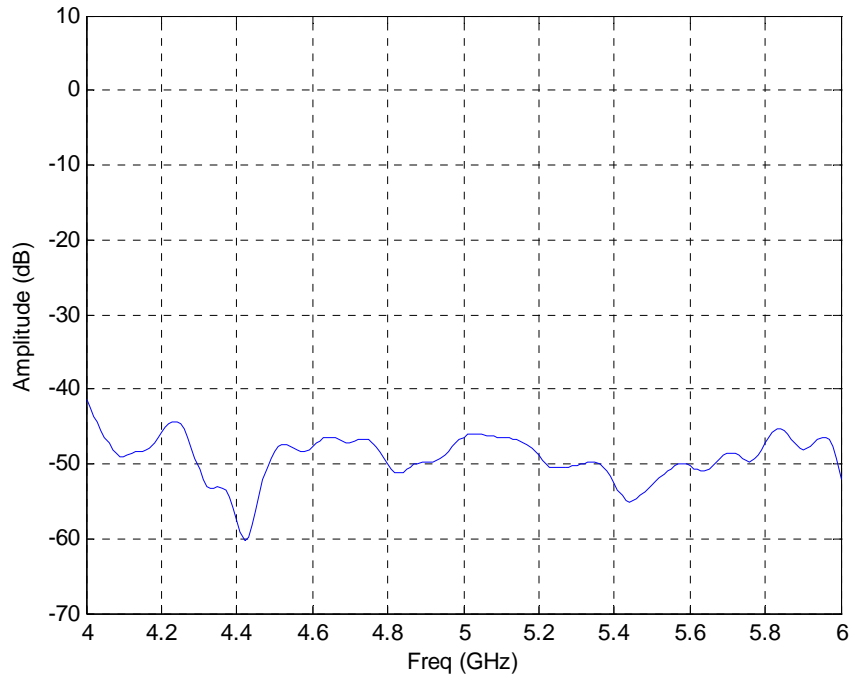


Figure 51. Ambient with time gate 25 – 40 ns, six meters from antenna

After doing a background subtraction, the 0.22 by 0.22 meter plate target is mounted on a wooden stand and placed onto the pedestal. The response of the plate with the time gate for six meters is shown in Figure 52. Compared to Figure 40, the plot with the time gate on shows a much larger residual of 15 to 20 dB above the average level.

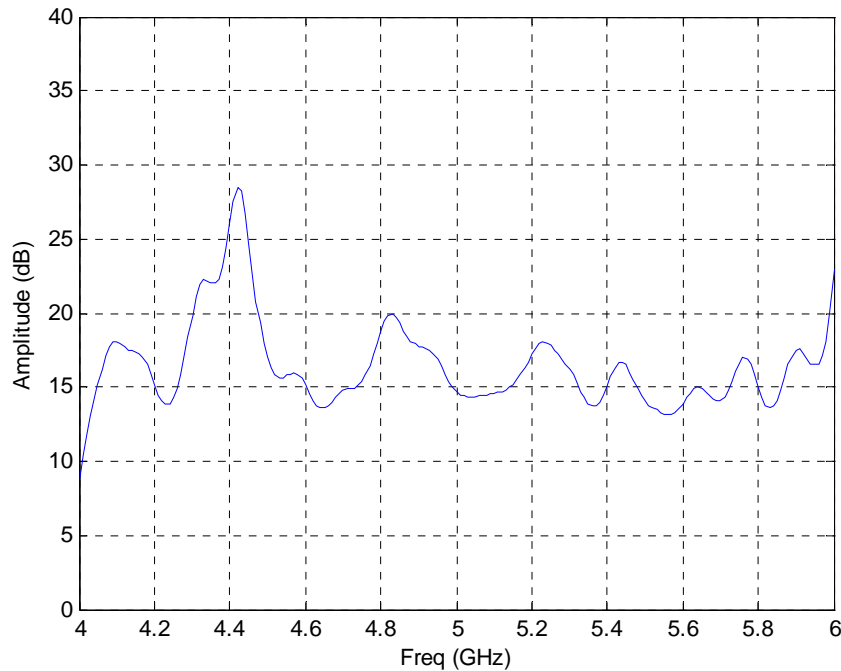


Figure 52. RCS of a 0.22 by 0.22 metal plate with time gate for six meters (with background subtraction)

In order to verify that the wooden stand did not affect the result, another measurement was conducted to compare the returns between the plate mounted on a wooden stand and the plate hanging from the ceiling on cloth string. The comparison result is shown in Figure 53. It shows that there is an insignificant difference between the plate on a wooden stand compared to the plate hanging down from the ceiling.

The next test was to measure the return of a wire hang vertically from the ceiling. The previous measurement without the time gate gives a maximum residual return of approximately 1 dB, shown in Figure 38. The measurement with the time gate at six meters from the antenna is shown in Figure 54.

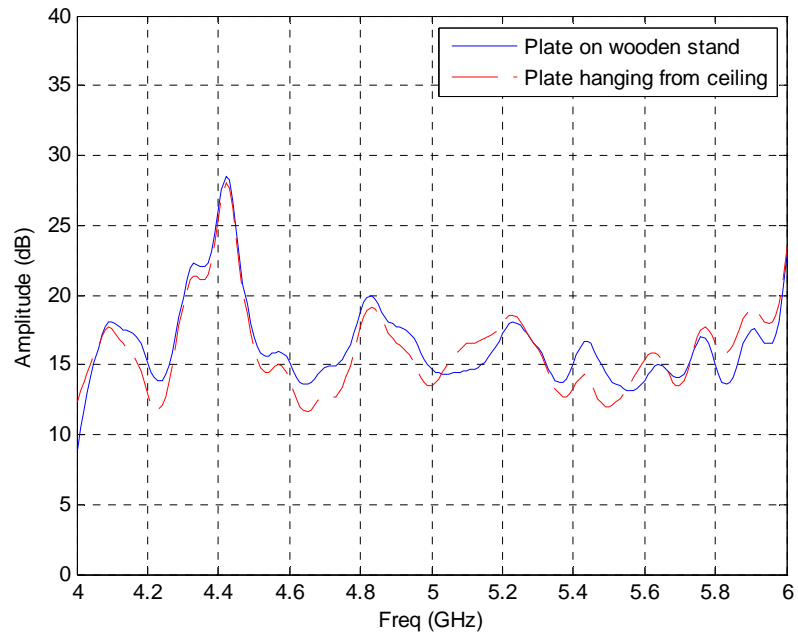


Figure 53. Comparison between plate on a wooden stand versus hanging from the ceiling, with time gate for six meters (with background subtraction)

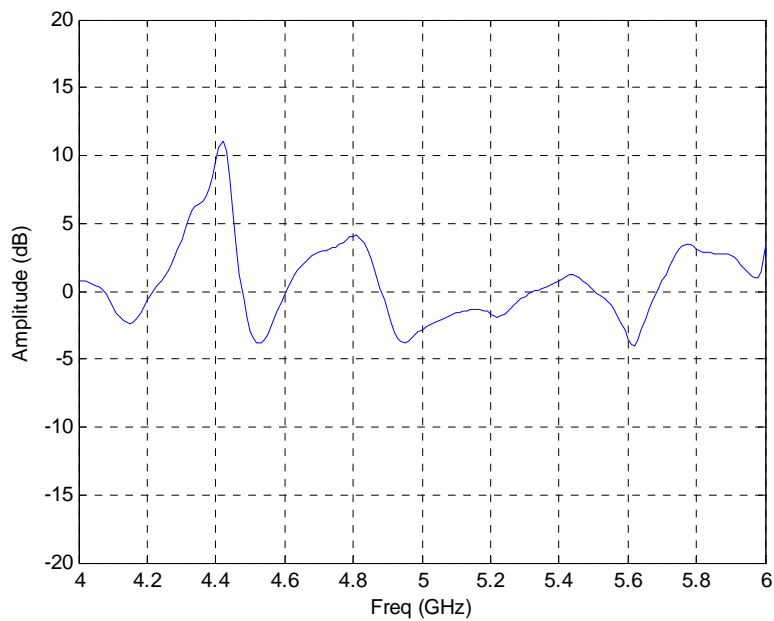


Figure 54. RCS of wire hang vertically from ceiling, with time gate for six meters (with background subtraction)

The result shows a somewhat better return than the 1 dB return without time gate. Although the multipath is eliminated by time gate, the 10 dB return of the wire is probably still too low to be picked up by the command wire sensor in a clutter environment.

### 3. Comparison Measurements

A plot was generated to compare the returns of three types of targets. Besides the previous two targets (the 0.22 by 0.22 meter plate and the wire), a third target (0.15 by 0.15 meter plate) was fabricated. The comparison plot is shown in Figure 55. The plot shows consistent characteristics, as well as the expected trend for the returns for the three targets. The 0.22 by 0.22 meter plate has the highest return, followed by the 0.15 by 0.15 meter plate. The wire has the lowest return.

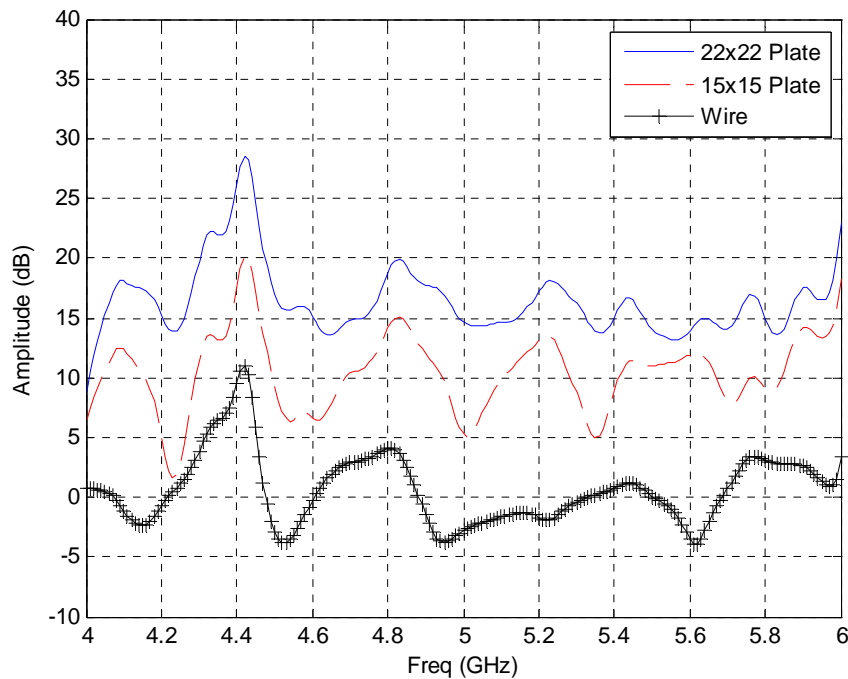


Figure 55. Comparison between three targets, with time gate on at six meters (with background subtraction)

In addition, it was necessary to determine the effect of the pedestal (located six meters from the antenna inside the anechoic chamber). The 0.22 by 0.22 meter plate was relocated to five meters away from the antenna, hanging down from the ceiling, as shown in Figure 56. The time gate was set from 20 to 30 ns, which corresponds to five meters from the antenna as listed in Table 4. In this way, the pedestal falls outside the time gate and does not contribute to the measurement.



Figure 56. A 0.22 by 0.22 meter plate five meters from the antenna

Two comparison plots were generated, one for the 0.22 by 0.22 meter plate and another for the wire hanging from the ceiling. They are shown in Figures 57 and 59, respectively. The photo of the wire hanging from the ceiling at five meters from the antenna is shown in Figure 58. From comparison of the two plots, it can be seen that the measurement for the time gate at five meters gives a higher return, approximately 20 dB higher for both cases, as compared the time gate at six meters. This proved that the pedestal at six meters does indeed lower the residual return of the target by at least 20 dB. Hence, subsequent measurements for the command wire sensor should be conducted at five meters or less from the antenna, in order to eliminate the effect of the pedestal on the readings.

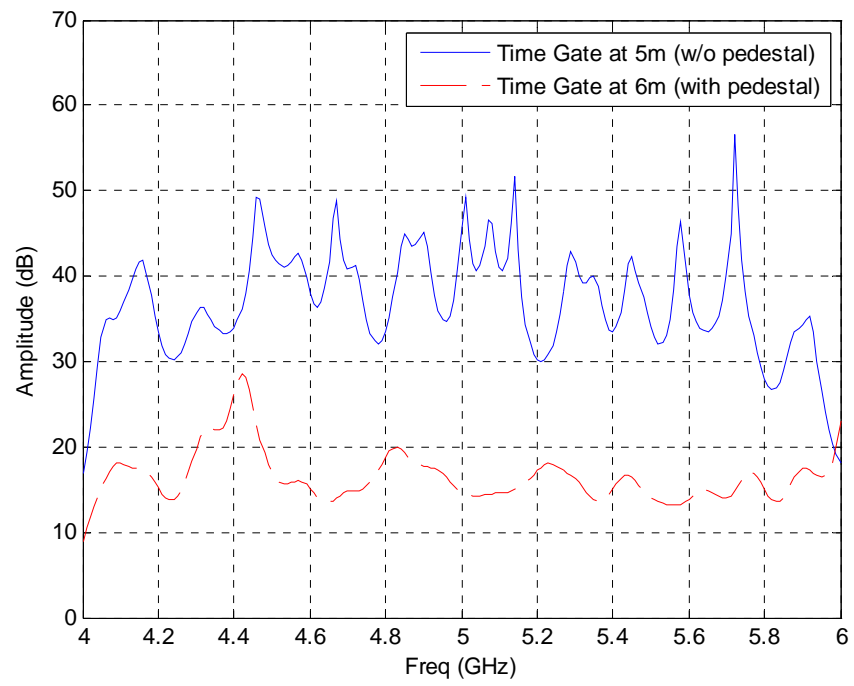


Figure 57. Comparison plot for 0.22 by 0.22 meter plate at five and six meters (with background subtraction)



Figure 58. Wire hang from ceiling, five meters from the antenna

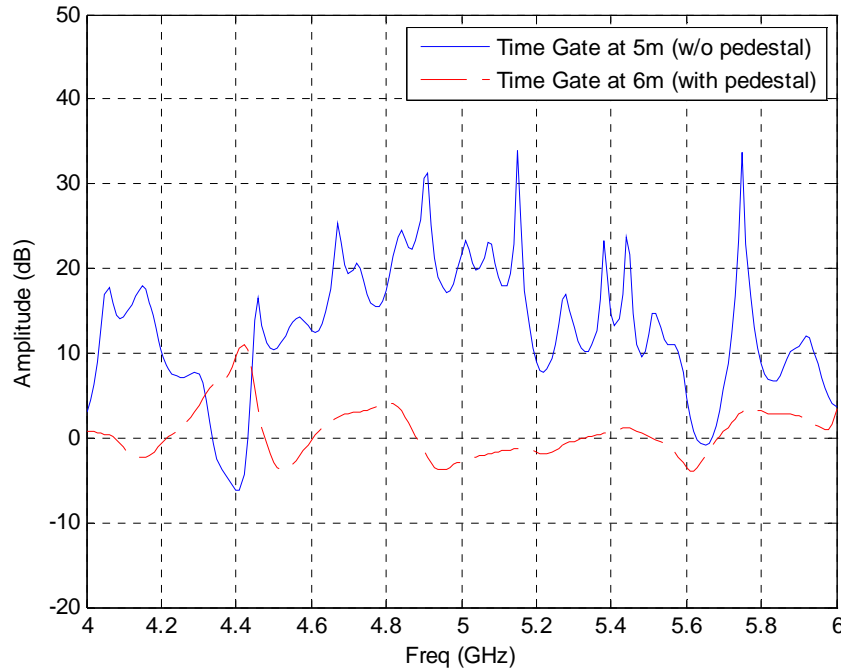


Figure 59. Comparison of returns for a wire hung from the ceiling, at five and six meters (with background subtraction)

#### 4. Comparison Measurements without Background Subtraction

All the previous measurements were done using background subtraction, meaning that after taking the ambient measurement, the background was subtracted out before putting the target into the chamber, and only the residual scattering was plotted. The comparison plot, which consists of the ambient, 0.22 by 0.22 meter plate and the wire, was generated and shown in Figure 60. The results show a significant 25 dB increase when the wire is introduced into the chamber, and there is another 20 dB difference between the wire and the metal plate. To better visualize and compare the difference, the average values over all frequencies were computed for each of the three targets and plotted in Figure 61. From the average plots, it can be seen that the scattering difference between ambient and the wire is 17.1 dB, and between the wire and plate is 21.6 dB. The differences are significant and can be used as a detection reference for the command wire sensor.



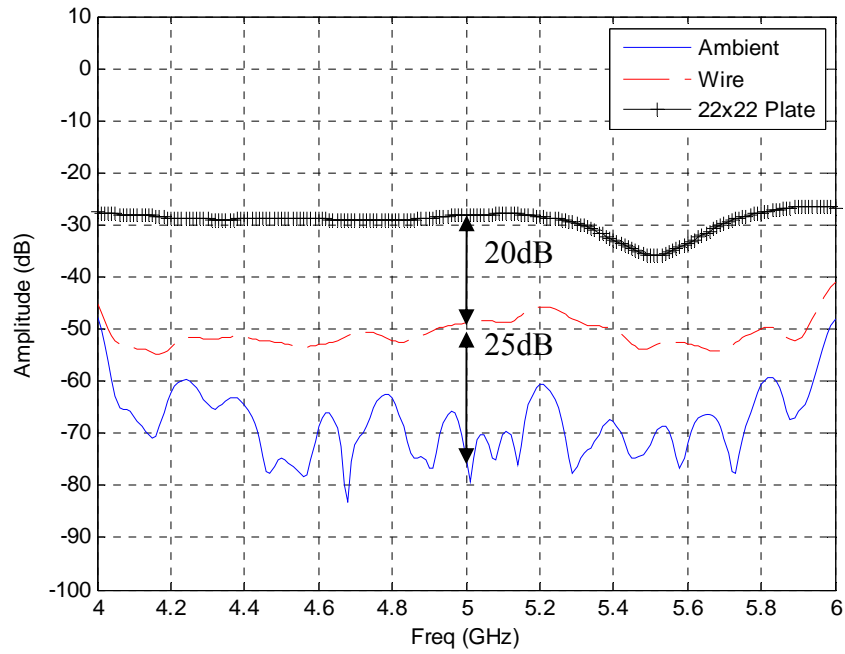


Figure 60. Comparison plots between the plate and wire, with time gate for five meters (without background subtraction)

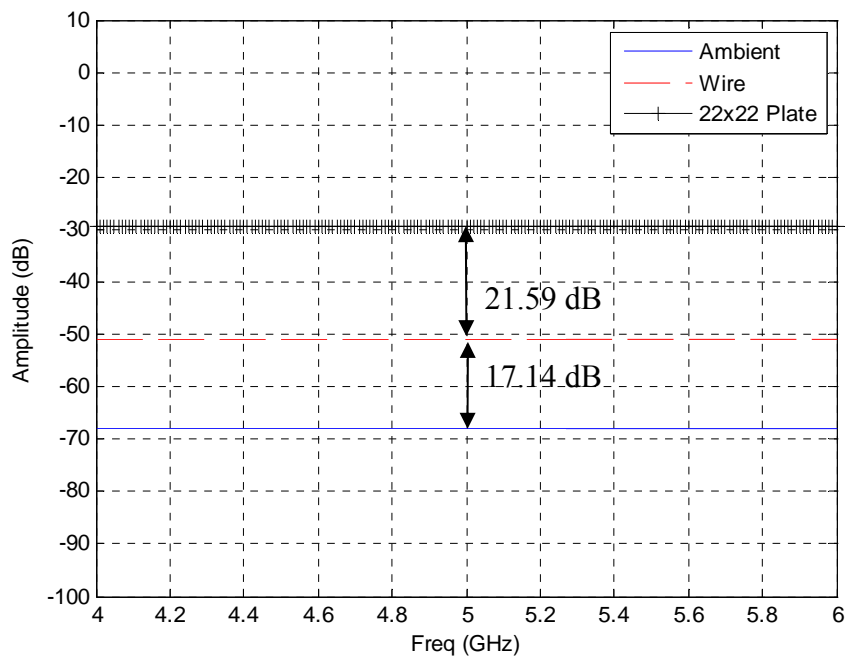


Figure 61. Frequency averaged scattering plots for the plate and wire (without background subtraction)

## 5. Wire Returns versus Aspect Angle without Background Subtraction

After obtaining the frequency averaged target scattering plot for detection reference, the next step was to examine the scattering differences for various aspect angles with time gating and without background subtraction. The comparison plot between a vertical wire and the ambient, with the time gate set at five meters and without background subtraction, is shown in Figure 62. The result shows approximately 10-15 dB difference between the ambient and the vertical wire residual.

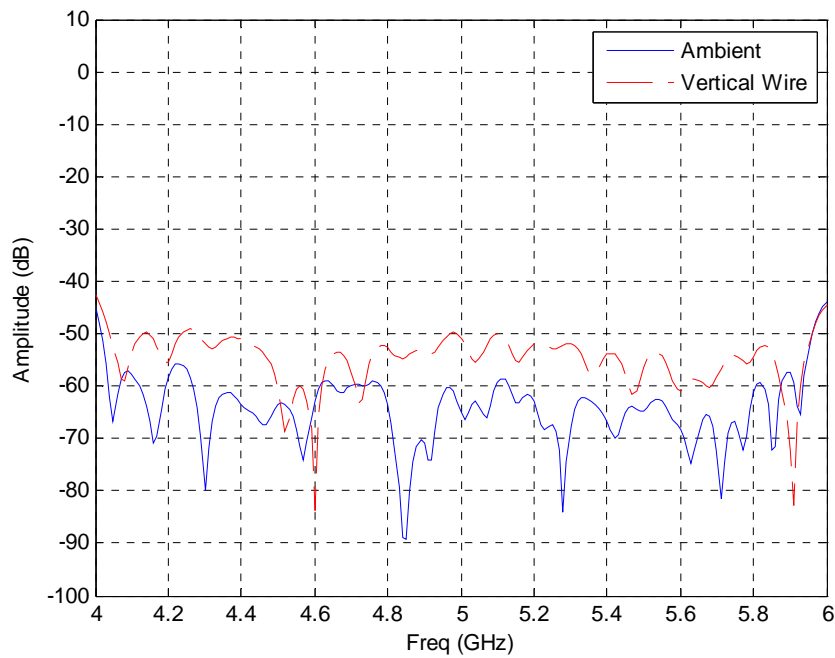


Figure 62. Comparison between vertical wire and ambient, with time gate for five meters (without background subtraction)

The next step was to place the wire horizontally at three different heights, as shown in Figures 63 and 64. This condition gives the wire return at various antenna tilt angles. The time gate is set from 20–30 ns, which corresponds to five meters away from the antennas.

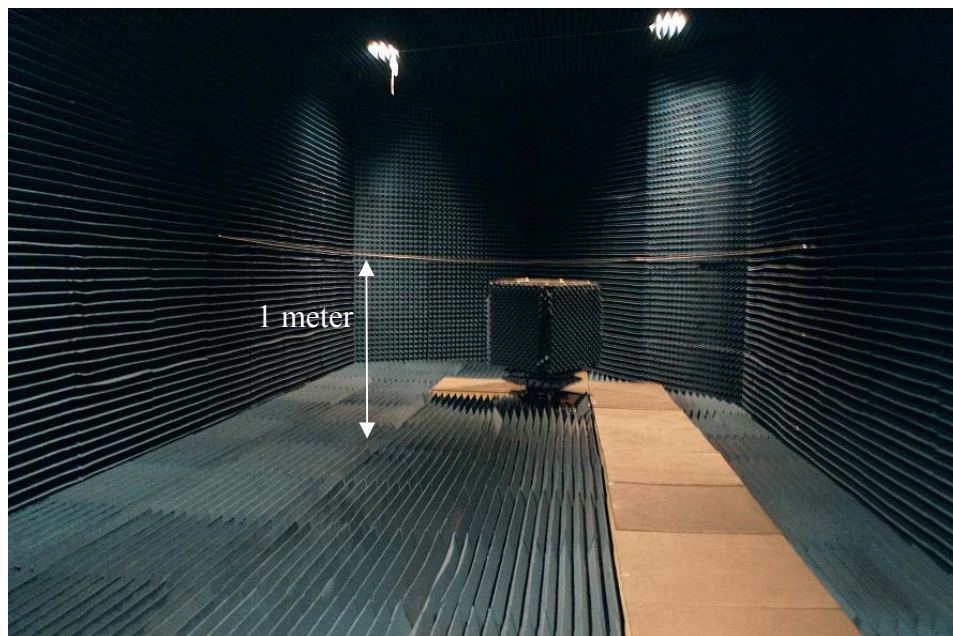


Figure 63. Horizontal wire placed one meter above the floor, five meters from the antenna

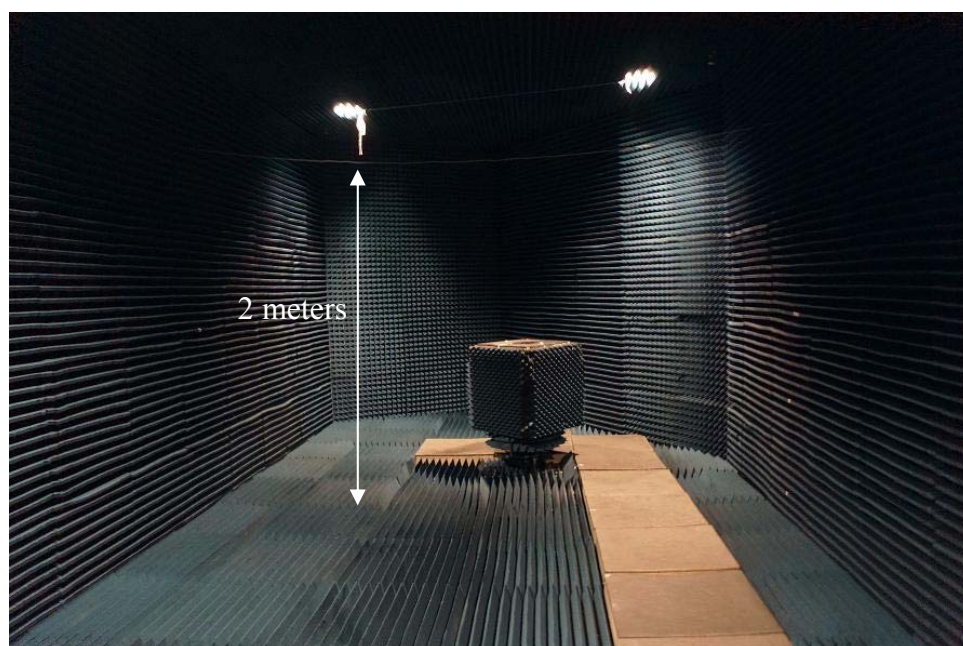


Figure 64. Horizontal wire placed two meters above the floor, five meters from the antenna

The measured data are shown in Figures 65, 66 and 67 for a horizontal wire on the floor, one meter height, and two meters height, respectively. The three plots show similar characteristics. The vertical wire return is consistently 10 dB higher than the horizontal wire return. The three different heights do not contribute any significant changes to the wire scattering returns. All of the measured horizontal wire returns are at the same level as the ambient. This is expected because the wire is completely cross polarized. Note that this situation would not occur for the sensor because it would use a circularly polarized antenna.

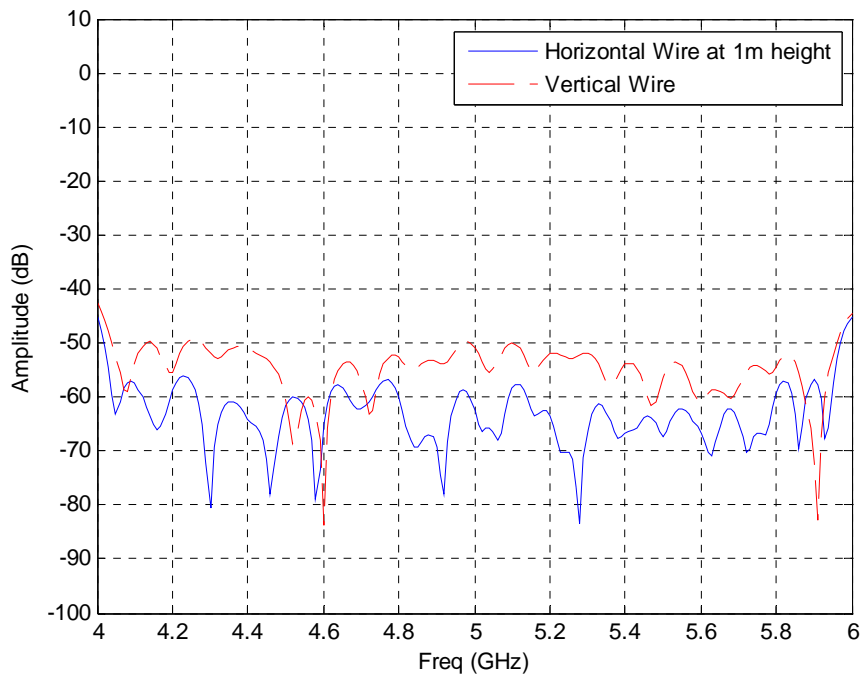


Figure 65. Comparison between vertical and horizontal wires at one meter height, with time gate for five meters (without background subtraction)

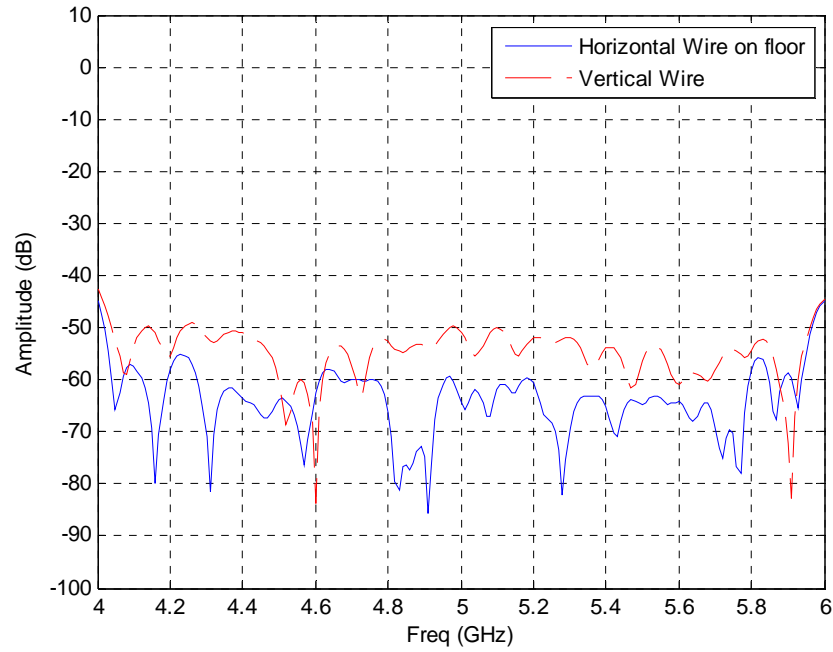


Figure 66. Comparison between vertical and horizontal wires on the floor, with time gate for five meters (without background subtraction)

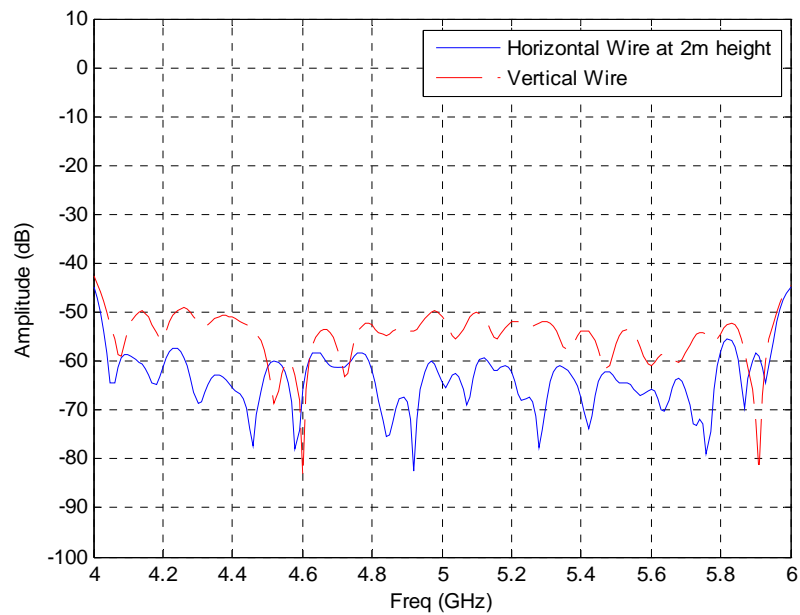


Figure 67. Comparison between vertical and horizontal wires at two meter height, with time gate for five meters (without background subtraction)

The next test was to measure the wire laid diagonally across the chamber, as shown in Figure 68. The diagonal wire was placed five meters away from the antenna, and the time gate was set from 20 – 30 ns. The measured scattering plot of the diagonal wire is shown in Figure 69. The vertical wire still gives a higher return than the diagonal wire, approximately 10-15 dB higher. Diagonal wire scattering return is slighter better than the horizontal wire. Therefore, the conclusion drawn from this test is that when the wire is aligned with the horn polarization, the scattering return will be the largest. There will always be a component of the electric field parallel to the wire axis if circular polarization is used.



Figure 68. Diagonal wire placed five meters from the antenna

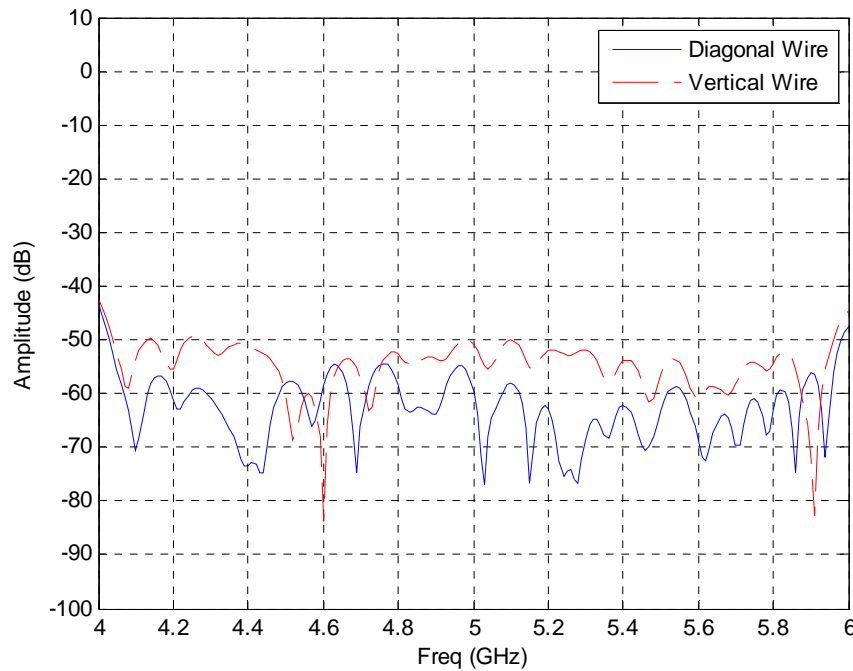


Figure 69. Comparison between vertical and diagonal wires, with time gate for five meters (without background subtraction)

Another measurement was conducted to determine the scattering return for vertical wires placed one meter to the left and right of the center of the main beam, as shown in Figures 70 and 71. The wire was hung vertically down from the ceiling, five meters from the antenna, one meter to the left and right of the main beam. The measured results are shown in Figures 72 and 73. From the two plots, the wire scattering return is slightly higher when the vertical wire is placed to the left of the main beam. This can be explained as the left and right walls of the anechoic chamber are not symmetrical. In addition, the transmit and receive horn is not located in the center of the chamber. As a result, there is more space to the left side of the chamber as compared to the right side of the chamber.



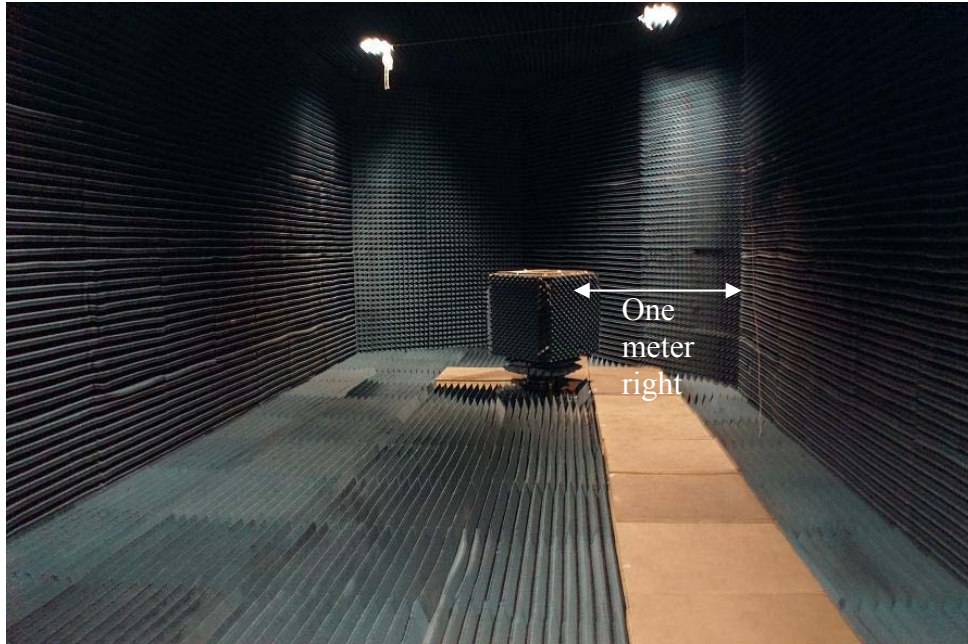


Figure 70. Vertical wire placed one meter right of main beam

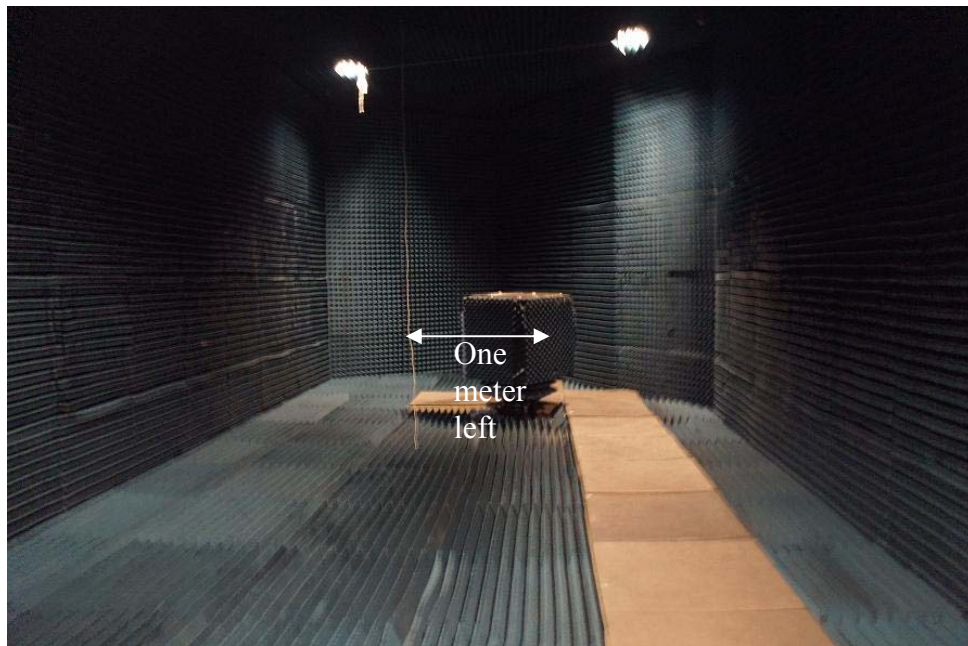


Figure 71. Vertical wire placed one meter left of main beam



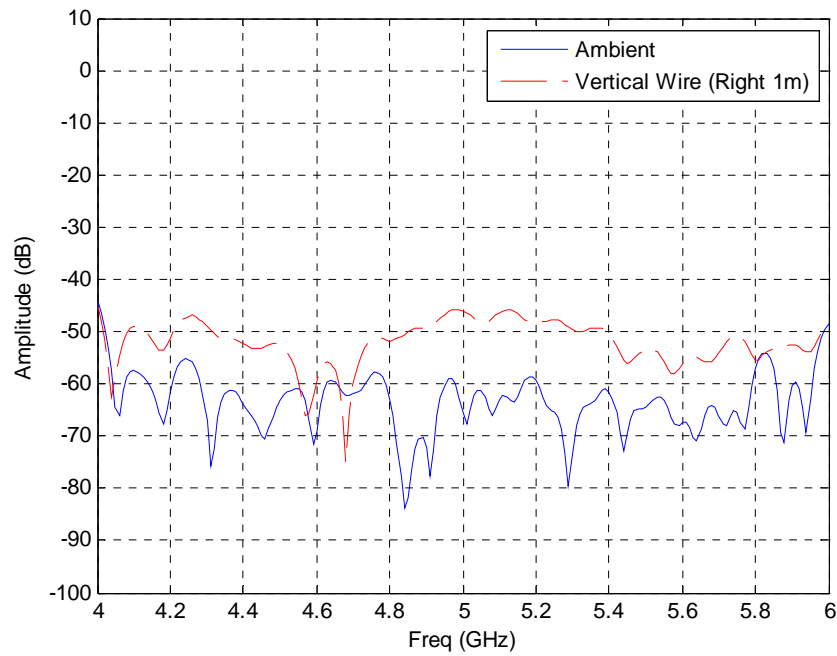


Figure 72. Comparison between ambient and vertical wire one meter to the right, with time gate for five meters (without background subtraction)

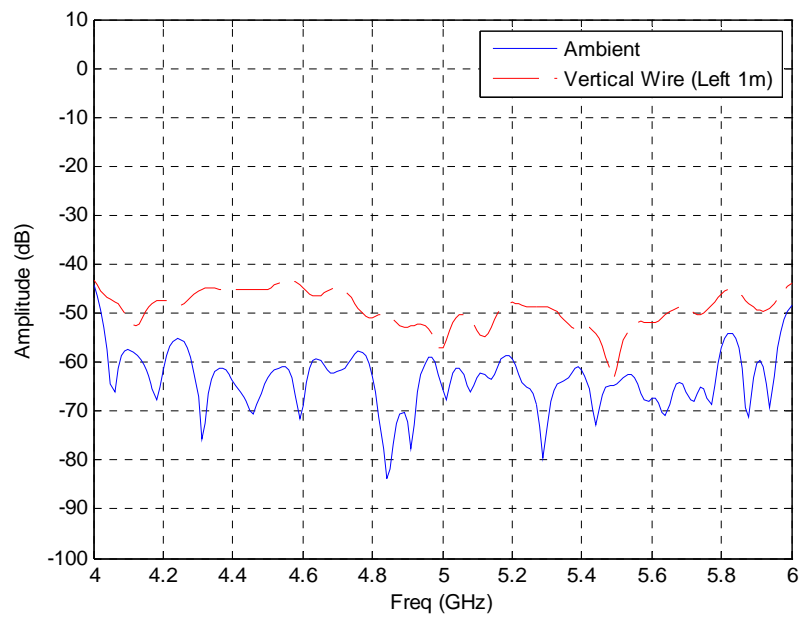


Figure 73. Comparison between ambient and vertical wire one meter to the left, with time gate for five meters (without background subtraction)

## **F. SUMMARY**

In summary, all the measurement procedures and results that were conducted for this thesis were presented in this chapter. The transmit-receive leakage was addressed, and the chamber multipath components were suppressed with time gating. Scattering between different types of targets was illustrated with various comparison plots. The most effective method for detecting the wire is to use circular polarization and do repeated frequency sweeps. A running average is kept, and when sweep's level exceeds a threshold based on the time history of averages, then the presence of a wire is declared. The summary, conclusions and recommendations for future work are presented in the next chapter.

## **V. SUMMARY, CONCLUSIONS AND RECOMMENDATIONS**

The summary and conclusions of the command wire sensor measurement results are covered in this chapter. Last, but not least, some recommendations for future work are presented.

### **A. SUMMARY AND CONCLUSIONS**

The focus of this thesis was to investigate the wire scattering behavior and clutter characteristics of the command wire sensor system. The theoretical aspects of wire scattering and clutter were covered in Chapter III. Basic equations were developed, so that fundamental relationships between system parameters could be examined.

After conducting the antenna beamwidth measurements, the first problem encountered was the transmit-receive leakage issue. The close proximity between the two horns causes some of the power to leak directly from the transmit horn to the receive horn. Further tests were conducted with various layers of absorber placed between the horns. Inserting two pieces of absorber reduced the leakage by 12 dB. As a result, for the command wire measurements, two pieces of absorber were used to reduce the leakage.

The initial wire measurements with background subtraction showed very low scattering returns, approximately in the range of 1 dB for wires laid on the ground as well as wires hung vertically from the ceiling. This level is not significant enough to be useful for a command wire sensor in a clutter environment. Hence, the next approach was to conduct a sensitivity measurement with a calibration target. After determining a plate dimension so that its HPBW would cover both antennas, a 0.22 by 0.22 meter metallic plate was fabricated. The metal plate measurements showed rapidly (in frequency) fluctuating peaks in the range of 3 to -6 dB. The measurement of a 3.2 meter metal pole also demonstrated similar fluctuating characteristics. Even though background subtraction is used, the conditions change once the target is placed in the chamber. The

fluctuations observed are due to the multiple reflections within the anechoic chamber, and interactions of the target with the chamber side walls, floor and ceiling. Therefore, time gating is required to eliminate the multipath components.

After determining the time gating period that corresponds to the distance within the chamber, the wire scattering measurements showed significant improvements in terms of a higher return (approximately 10 dB). The next approach was to eliminate the effect of the pedestal in the measurement results. The wire was measured at five meters from the antenna with time gating, such that the pedestal is out of the time gate. The result showed an improved 30 dB return, proving that the pedestal does indeed lower the scattering returns of the target by at least 20 dB.

The next approach was to compare the measurements with and without background subtraction. Without background subtraction, the average plots showed a scattering difference of 17.1 dB between ambient and the wire, as well as a 21.6 dB between the wire and the plate. Measurements between different horizontal, vertical and diagonal wires were also presented. From the results, it is clear that the wire scattering return is the highest when the wire is aligned with the horn polarization. There is always a component parallel to the wire if circular polarization is used in the sensor system.

In conclusion, this research has addressed several technical challenges with regards to the command wire sensor. The significant transmit-receive coupling was identified, and leakage reduction was resolved. Various wire scattering and clutter characteristics were illustrated with the measurements. The theoretical calculations were also validated with actual measurements. Last, but not least, the measurements have demonstrated close-in clutter rejection by utilizing time gating.

## **B. RECOMMENDATIONS**

Further efforts can be explored to gather more in-depth measurements for the command wire sensor. Due to the anechoic chamber limitations, there were some tests that could not be performed. It would be extremely beneficial if the anechoic chamber can be further modified so that a more accurate wire scattering can be achieved. The transmit and receive antenna separation needs to increase so as to reduce transmit-receive

coupling. Further tests can be conducted to identify the optimal distance between the two horns. The antenna mount should also be redesigned to be able to tilt upwards and downwards, so that the antenna can be tilted down to face the floor, where the command wire is typically located.

In addition, the main problem within the anechoic chamber was mounting the target at various desired locations and aspect angles. Hence, a recommendation is to incorporate accessible target mounting fixtures at various distances from the antenna as well as extend the chamber walkway in order to access these locations. Lastly, it would also be interesting to conduct outdoor measurements for the command wire sensor, as the outdoor environment will be very different and challenging as compared to the controlled chamber environment.

THIS PAGE INTENTIONALLY LEFT BLANK

## LIST OF REFERENCES

- [1] Wikipedia. (n.d.). *Improvised explosive device* [online encyclopedia]. Available: [http://en.wikipedia.org/wiki/Improvised\\_explosive\\_device](http://en.wikipedia.org/wiki/Improvised_explosive_device) [Accessed August 20, 2012].
- [2] BBC News. (2009, December 14). *Growing Menace of Afghan IEDs* [online]. Available: [http://news.bbc.co.uk/2/hi/south\\_asia/8136266.stm](http://news.bbc.co.uk/2/hi/south_asia/8136266.stm) [Accessed August 20, 2012].
- [3] R. C. Matson, (2011, January 6). *Red Bulls patrol IED hotbed* [online]. Available: <http://iowaredbulls.armylive.dodlive.mil/2011/01/06/red-bulls-patrol-ied-hotbed/>. [Accessed August 20, 2012].
- [4] D. J. Daniels, *Ground Penetrating Radar*, Institution of Engineering and Technology, 2004.
- [5] Naval Surface Warfare Center Dahlgren, Public Affairs. (2011, November 17). *Navy Scientists Discoverd IED Detection Techniques* [online]. Available: [http://www.navy.mil/submit/display.asp?story\\_id=63879](http://www.navy.mil/submit/display.asp?story_id=63879). [Accessed August 20, 2012].
- [6] Wikipedia. (n.d.). *Synthetic aperture radar* [online encyclopedia]. Available: [http://en.wikipedia.org/wiki/Synthetic\\_aperture\\_radar](http://en.wikipedia.org/wiki/Synthetic_aperture_radar) [Accessed August 20, 2012].
- [7] D. C. Jenn, "Command Wire Sensor," Naval Postgraduate School, Monterey California, 2009.
- [8] G. Zorpette, (2008, September). *Countering IEDs* [online]. Available: <http://spectrum.ieee.org/aerospace/military/countering-ieds/7>. [Accessed August 20, 2012].
- [9] D. Larter, (2010, June 26). *Army turns to Huskies to fight against IEDs* [online]. Available: [http://www.armytimes.com/news/2010/06/army\\_husky\\_062610w/](http://www.armytimes.com/news/2010/06/army_husky_062610w/). [Accessed August 20, 2012].
- [10] Online Show Daily News DSEI 2011. (2011, July 18). *Land Systems at DSEI 2011* [online]. Available: [http://www.armyrecognition.com/dsei\\_2011\\_daily\\_news\\_actualites\\_pictures\\_video\\_uk/static\\_vehicle\\_land\\_systems\\_park\\_makes\\_its\\_debut\\_at\\_defence\\_exhibition\\_in\\_london\\_dsei\\_2011.html](http://www.armyrecognition.com/dsei_2011_daily_news_actualites_pictures_video_uk/static_vehicle_land_systems_park_makes_its_debut_at_defence_exhibition_in_london_dsei_2011.html). [Accessed August 20, 2012].
- [11] Wikipedia. (n.d.). *Brewster's angle* [online encyclopedia]. Available: [http://en.wikipedia.org/wiki/Brewster's\\_angle](http://en.wikipedia.org/wiki/Brewster's_angle) [Accessed August 20, 2012].

- [12] F. Ulaby, *Fundamentals of Applied Electromagnetics*, Pearson Prentice Hall, 5<sup>th</sup> Edition, 2007.
- [13] C. Wolf. (n.d.). *Radar Basics – Synthetic Aperture Radar* [online tutorial]. Available: <http://www.radartutorial.eu/20.airborne/ab07.en.html>. [Accessed August 20, 2012].
- [14] M. Skolnik, *Introduction to Radar Systems*, McGraw Hill, 3<sup>rd</sup> Edition.
- [15] Security International's News Correspondent. (2011, November 22) *US Navy Unveils Radar IED Detection Method* [online]. Available: <http://www.security-technologynews.com/news/us-navy-unveils-radar-ied-detection-method.html>. [Accessed August 20, 2012].
- [16] T. Lively. (2012, April 4) *Change Detection – Warfighters finally have a “Cheat-Sheet”* [online]. Available: <http://sofrep.com/5207/change-detection-warfighters-cheat-sheet/> [Accessed August 20, 2012].
- [17] C. Butler, “The Equivalent Radius of a Narrow Conducting Strip,” *IEEE Trans. on Antennas and Prop.*, vol. AP-30, no. 4, pp. 755-758, 1982.
- [18] D. C. Jenn, Lecture notes for EC4630, Radar and Laser Cross Section, Naval Postgraduate School, 2012 (unpublished).
- [19] H. Shamansky, A. Dominek, L. Peters, “Electromagnetic Scattering by a Straight Thin Wire,” *IEEE Trans. on Antennas and Prop.*, vol. 37, no. 8, pp. 1019-1025, 1989.
- [20] D. C. Jenn, Lecture notes for EC3630, Propagation near the Earth's Surface, Naval Postgraduate School, 2012 (unpublished).
- [21] B. Erenoglu, “Naval Postgraduate School Anechoic Chamber Evaluation,” Naval Postgraduate School, September 2004.
- [22] D. C. Jenn, *Radar and Laser Cross Section Engineering*, American Institute of Aeronautics and Astronautics, 2<sup>nd</sup> Edition, 2005.



## **INITIAL DISTRIBUTION LIST**

1. Defense Technical Information Center  
Ft. Belvoir, Virginia
2. Dudley Knox Library  
Naval Postgraduate School  
Monterey, California
3. Professor R. Clark Robertson  
Chairman, Department of Electrical & Computer Engineering  
Naval Postgraduate School  
Monterey, California
4. Professor David C. Jenn  
Professor, Department of Electrical & Computer Engineering  
Naval Postgraduate School  
Monterey, California
5. Professor Tri T. Ha  
Professor, Department of Electrical & Computer Engineering  
Naval Postgraduate School  
Monterey, California
6. Robert D. Broadston  
Staff, Department of Electrical & Computer Engineering  
Naval Postgraduate School  
Monterey, California
7. Professor Tat Soon Yeo  
Director, Temasek Defense Systems Institute (TDSI)  
National University of Singapore  
Singapore
8. Ms. Lai Poh Tan  
Senior Manager, Temasek Defense Systems Institute (TDSI)  
National University of Singapore  
Singapore
9. Mr. Saik Hay Fong  
Chief Technology Officer, ST Engineering  
Singapore

10. Mr. Richard Kwok  
Chief Technology Officer, ST Kinetics  
Singapore
11. Mr. Leng Seng Ang  
Vice President, ST Kinetics  
Singapore
12. Mr. Chin Liong Yeo  
Principal Engineer, ST Kinetics  
Singapore